Vincent, E. E., Sergushichev, A., Griss, T., Gingras, M. C., Samborska, B., Ntimbane, T., Coelho, P. P., Blagih, J., Raissi, T. C., Choinière, L., Bridon, G., Loginicheva, E., Flynn, B. R., Thomas, E. C., Tavaré, J. M., Avizonis, D., Pause, A., Elder, D. J. E., Artyomov, M. N., & Jones, R. G. (2015). Mitochondrial Phosphoenolpyruvate Carboxykinase Regulates Metabolic Adaptation and Enables Glucose-Independent Tumor Growth. *Molecular Cell*, *60*(2), 195-207. https://doi.org/10.1016/j.molcel.2015.08.013

Peer reviewed version

Link to published version (if available):
10.1016/j.molcel.2015.08.013

Mitochondrial phosphoenolpyruvate carboxykinase (PCK2) regulates metabolic adaptation and enables glucose-independent tumor growth

Emma E. Vincent[1,2], Alexey Sergushichev[3,4], Takla Griss[1,2], Marie-Claude Gingras[1,5], Bozena Samborska[1,2], Thierry Ntimbane[1,6], Paula P. Coelho[1,2], Julianna Blagih[1,2], Thomas C. Raissi[1,2], Luc Choinière[1,6], Gaëlle Bridon[1,6], Ekaterina Loginicheva[4], Breanna R. Flynn[1,2], Elaine C. Thomas[7], Jeremy M. Tavaré[7], Daina Avizonis[1,6], Arnim Pause[1,5], Douglas J.E. Elder[7], Maxim N. Artyomov[4,*] and Russell G. Jones[1,2,*]

Author Affiliation: [1]Goodman Cancer Research Centre, McGill University, Montreal, QC, H3A 1A3, Canada; [2]Department of Physiology, McGill University, Montreal, QC, H3G 1Y6, Canada; [3]ITMO University, Saint Petersburg, 197101, Russia; [4]Department of Pathology and Immunology, Washington University in St Louis, St Louis, Missouri, 63110, USA; [5]Department of Biochemistry, McGill University, Montreal, QC, H3G 1Y6, Canada; [6]Metabolomics Core Facility, Goodman Cancer Research Centre, McGill University, Montreal, QC, H3A 1A3, Canada; [7]School of Biochemistry, Medical Sciences Building, University of Bristol, BS8 1TD, United Kingdom.

***Corresponding authors:** Russell G. Jones, Goodman Cancer Research Centre, Department of Physiology, McGill University, 3655 Promenade Sir William Osler, Room 705, Montreal, Quebec, H3G 1Y6, CANADA. Email: russell.jones@mcgill.ca,

Phone: (514) 398-3336, Fax: (514) 398-6769; Maxim N. Artyomov, Department of Pathology and Immunology, Division of Immunobiology, Washington University School of Medicine, 660 S. Euclid Avenue, Campus Box 8118, St. Louis, MO 63110, USA. Email: martyomov@pathology.wustl.edu, Phone: (314) 286-2951.

Running title: PCK2 supports glucose-independent tumor growth

Summary

Cancer cells adapt metabolically to proliferate under nutrient limitation. Here we used combined transcriptional-metabolomic network analysis to identify metabolic pathways that support glucose-independent tumor cell proliferation. We found that glucose deprivation stimulated re-wiring of the tricarboxylic acid (TCA) cycle and early steps of gluconeogenesis to promote glucose-independent cell proliferation. Glucose limitation promoted the production of phosphoenolpyruvate (PEP) from glutamine via the activity of mitochondrial PEP-carboxykinase (PCK2). Under these conditions, glutamine-derived PEP was used to fuel biosynthetic pathways normally sustained by glucose, including serine and purine biosynthesis. PCK2 expression was required to maintain tumor cell proliferation under limiting glucose *in vitro* and tumor growth *in vivo*. Elevated *PCK2* expression is observed in several human tumor types and enriched in tumor tissue from non-small-cell lung cancer (NSCLC) patients. Our results define a role for PCK2 in cancer cell metabolic reprogramming that promotes glucose-independent cell growth and metabolic stress resistance in human tumors.

Introduction

One of the primary metabolic phenotypes observed in transformed cells is an increase in aerobic glycolysis (the "Warburg Effect"), which is marked by increased glucose uptake and lactate production. Glucose is used to generate ATP via glycolysis or mitochondrial oxidative phosphorylation (OXPHOS) (DeBerardinis et al., 2008a), while glycolytic intermediates also function as key substrates for macromolecular biosynthesis, supplying carbon for the synthesis of non-essential amino acids (NEAAs), intermediates of one-carbon metabolism, nucleotides, and lipids (Locasale, 2013; Lunt and Vander Heiden, 2011). Another key nutrient for proliferating cancer cells is the NEAA glutamine. Proliferating cells maintain TCA cycle function using glutamine as an anapleurotic substrate to generate mitochondrial α-ketoglutarate (α-KG) and subsequent biosynthetic intermediates (DeBerardinis et al., 2007). Glutamine enables the TCA cycle to function both as a carbon source for ATP production and a biosynthetic hub (Ahn and Metallo, 2015; Deberardinis et al., 2008b).

Much of our understanding of tumor cell metabolism is based on the metabolic programs engaged by cancer cells *in vitro*, where nutrient availability is in excess. However, glucose concentrations in tumors can be limiting - 3- to 10-fold lower than in non-transformed tissues (Birsoy et al., 2014; Hirayama et al., 2009) - due to a combination of reduced tumor vascularization and high rates of glucose consumption by cancer cells. Thus, tumor cells must enact strategies to grow and survive in metabolically unfavorable environments.

Under limited glucose, cells capable of engaging OXPHOS have greater capacity to proliferate (Birsoy et al., 2014; Chen et al., 2015). Glutamine can partially compensate for glucose to maintain TCA cycle function under conditions of

metabolic stress. Acetyl-CoA can be generated from glutamine through reductive carboxylation of α-KG under conditions of hypoxia or reduced mitochondrial function (Metallo et al., 2012; Mullen et al., 2012; Wise et al., 2011). Similarly, TCA cycle function is maintained in glucose-deprived cells in part through the production of glutamine-derived pyruvate, which can be converted to acetyl-CoA and oxidized by mitochondria (Blagih et al., 2015; Le et al., 2012; Yang et al., 2014; Yang et al., 2009). However, efficiency of OXPHOS and TCA cycle maintenance cannot fully account for cell proliferation under glucose limitation, as glycolytic intermediates are still required to generate biosynthetic precursors essential for cell division.

Here we have used metabolomic and transcriptional profiling to characterize pathways of glucose-independent tumor cell growth. Using this systems-level analysis, we have identified alterations in glutamine metabolism and the early steps of gluconeogenesis as key metabolic adaptations for tumor cells to proliferate under low glucose conditions. Here we describe a role for mitochondrial phosphoenolpyruvate (PEP) carboxykinase (PEPCK-M or PCK2) in mediating tumour cell adaptation to glucose limitation that facilitates tumor growth *in vivo*.

Results

Network-based data integration reveals distinct metabolic nodes in tumor cells adapted to glucose-independent proliferation

To gain insight into how cellular proliferation can be maintained under glucose-free conditions, we examined the growth of the NSCLC cell lines A549 and H1299, which are capable of proliferating in medium lacking glucose, but not glutamine (Figure 1A). We performed a systems-level analysis of intracellular metabolites isolated from A549 cells cultured for 48 hours in the absence of glucose. The relative metabolite abundance in glucose-starved A549 cells is shown in Figure S1. Metabolite set enrichment analysis (MSEA) of these data revealed enrichment in metabolites involved in amino acid degradation (ammonia cycling, urea cycle), the TCA cycle, glutamate metabolism, and gluconeogenesis (Figure 1B). We next integrated RNA-seq-based transcriptional profiling with our metabolic profiling data to construct a network-based analysis of possible metabolic fluxes (Jha et al., 2015). To trace all possible metabolic transformations of the labeled atoms, we constructed a metabolic network where individual nodes are individual carbon atoms connected by edges (connecting lines) corresponding to chemical reactions (totaling to about 30,000 edges). From this we identified a sub-network based on connectivity and changes in metabolite abundance and metabolic enzyme gene expression under conditions of glucose deprivation (Figure 1C).

From this network-based analysis we identified five major metabolic modules differentially regulated in A549 cells undergoing glucose-independent proliferation: glycolysis, the TCA cycle, glutamate/proline metabolism, inositol metabolism and serine metabolism (Figure 1C). Nodes for glycolysis and lactate production were, as

expected, significantly downregulated in A549 cells cultured under glucose-free conditions. Conversely, genes involved in inositol and proline metabolism were selectively upregulated under glucose withdrawal, while the intracellular concentration of several amino acids (serine, aspartate, asparagine, tryptophan and glycine) was also elevated. MSEA revealed enrichment in metabolites involved in glutamate metabolism and gluconeogenesis (Figure 1B). This is noteworthy because glutamine is a known gluconeogenic substrate (Stark and Kibbey, 2014). There is increased transamination of glutamate to α-KG (through ASNS and BCAT1), which is consistent with the increased glutamine dependence of A549 cells. The network also highlighted a significant upregulation in the conversion of oxaloacetate (OAA) to both aspartate (via GOT1) and PEP (via the gluconeogenic enzyme PCK2). Finally, increased levels of serine and glycine were coupled with transcriptional upregulation of PHGDH, an enzyme that directs glycolytic intermediates towards the serine biosynthesis pathway (Locasale, 2013). Taken together these data suggest an active role for glutamine as both a carbon and nitrogen source for amino acid metabolism, which may be achieved through the malate-aspartate shuttle and early steps of gluconeogenesis under low glucose conditions.

Glutamine maintains TCA cycle metabolism and levels of the glycolytic intermediate PEP under glucose-free conditions

Our transcriptional-metabolic network analysis indicated increased levels of glutamine metabolism in A549 cells proliferating in the absence of glucose. To characterize how glutamine is metabolized under glucose-free conditions, A549 cells were cultured in the presence of uniformly labeled ^{13}C glutamine (U-[^{13}C]-Q). Conventional metabolism of U-[^{13}C]-glutamine in tumor cells is illustrated in Figure

2A. Similar ^{13}C-labeling patterns were observed in glutamate and TCA cycle intermediates (α-KG, succinate, fumarate, and malate) under glucose-free and glucose-replete conditions (Figure 2B), indicating that glutamine continues to be used as an anaplerotic substrate for the TCA cycle when glucose is limiting. Levels of ^{13}C-glutamine-derived glutamate, succinate, and aspartate were increased under glucose withdrawal conditions, while the levels of many of the TCA cycle metabolites decreased under glucose withdrawal (Figure S2A), consistent with the network analysis in Figure 1C.

Citrate production from glutamine was strikingly altered in A549 cells under glucose withdrawal. We observed a significant increase in the proportion of the citrate pool labeled from U-[^{13}C]-glutamine, as shown by the large decrease in unlabeled citrate under glucose-free conditions (Figure 2C). The increased labeling of citrate from U-[^{13}C]-glutamine was due to increases in both reductive carboxylation of α-KG (m+5 citrate) and the emergence of a fully labeled citrate molecule (m+6 citrate) (Figure 2C). Levels of m+6 citrate were negligible in A549 cells grown in the presence of glucose, but had not yet reached steady-state levels after 6 hours of labeling with U-[^{13}C]-glutamine under glucose-free conditions (Figure 2D).

Formation of m+6 citrate can occur if U-[^{13}C]-glutamine is used to generate both OAA and acetyl-CoA, the latter requiring the formation of m+3 pyruvate from ^{13}C-glutamine (Figure S2B). It has been shown previously that the decarboxylation of glutamine-derived malate (m+4) can generate pyruvate m+3 through the activity of the malic enzyme (Guay et al., 2007; Yang et al., 2014). Alternatively, PEPCK can generate PEP (m+3) from OAA, followed by conversion of PEP to pyruvate by pyruvate kinase (PK). We found that while the overall abundance of pyruvate was lower in A549 cells growing in glucose-free conditions, the majority of pyruvate

(m+3) in these cells was derived from ^{13}C-glutamine (Figure 2E). In addition, we observed a significant increase in U-[^{13}C]-glutamine-derived PEP specifically in A549 cells growing under glucose-free conditions (Figure 2F).

Consistent with the network analysis (Figure 1C), lactate production was significantly downregulated in glucose-starved A549 cells (Figure S2C), and U-[^{13}C]-glutamine was not used for its synthesis. In contrast, glutamine was used in the synthesis of both pyruvate and PEP (Figure S2D). H1299 cells displayed similar increases in m+6 citrate, m+3 pyruvate, and m+3 PEP derived from ^{13}C-glutamine specifically when growing under conditions of glucose withdrawal (Figure 2G). The presence of pyruvate m+3 and citrate m+6 suggests these cells are undergoing pyruvate cycling (Yang et al., 2014), using glutamine to maintain TCA function when glucose is unavailable.

PCK2 is required for the production of glutamine-derived PEP

Our RNA-seq results indicated that expression of the mitochondrial form of PEPCK (*PCK2*) was increased in A549 cells upon glucose withdrawal. However, no sequencing reads for *PCK1*, the cytosolic form of PEPCK, were detected (data not shown). Consistent with this, silencing *PCK1* in A549 cells did not affect total PEPCK protein levels (Figure S3A). These data suggest that PCK2 is the sole PEPCK isoform expressed in A549 cells, in agreement with recent findings (Leithner et al., 2014).

We next investigated the role of PCK2 in glutamine metabolism by silencing PCK2 expression in A549 and H1299 cells using RNA interference (Figure 3A) or 3-mercaptopicolinic acid (MPA), a specific inhibitor of PEPCK activity (Urbina et al., 1990). Conversion of U-[^{13}C]-glutamine to PEP (Figure 3B) was stimulated by

glucose deprivation as before, but was markedly reduced in cells expressing *PCK2* shRNA or treated with MPA (Figure 3C). Glutamine flux into PEP was also ablated in glucose-starved A549 cells expressing *PCK2* shRNA (Figure S3B). This effect appeared to be specific to the formation of PEP, as inhibiting PCK2 did not significantly affect TCA cycle anaplerosis from glutamine in A549 cells regardless of glucose availability (Figure S3C).

To address whether PCK2 contributed to pyruvate cycling in A549 cells growing under glucose limitation (schematic in Figure 3B), we measured the formation of m+3 pyruvate (Figure 3D) and m+6 citrate (Figure S3D) in cells expressing *PCK2* shRNA. A549 cells expressing *PCK2* shRNA displayed reduced labeling of pyruvate (m+3, Figure 3D) and citrate (m+6, Figure S3D) from U-[^{13}C]-glutamine specifically under conditions of glucose withdrawal. Similarly, MPA treatment reduced the production of m+3 pyruvate from U-[^{13}C]-glutamine in A549 cells growing in the absence of glucose (Figure 3D).

Glutamine-derived PEP is used as a biosynthetic intermediate under low glucose conditions

The reduced labeling of m+3 pyruvate and m+6 citrate upon PCK2 inhibition (Figure 3D and S3D) was modest compared to the large reduction in m+3 PEP observed in NSCLC cells expressing *PCK2* shRNA (Figure 3C), suggesting that glutamine-derived PEP may be formed for a purpose other than pyruvate cycling. Our network analysis indicated a specific increase in the serine biosynthesis pathway in glucose-deprived A549 cells (Figure 1C). Therefore, we assessed ^{13}C enrichment in serine and glycine in A549 cells cultured with U-[^{13}C]-glutamine under glucose-free conditions. ^{13}C-glutamine-derived carbon was detected in serine (Figure 4A and S4A) and glycine

(Figure 4B and S4A) from A549 cells undergoing glucose-independent proliferation. H1299 cells demonstrated a similar shift towards glutamine-dependent serine and glycine biosynthesis under glucose-free conditions, indicating that glutamine can substitute for glucose as a carbon source for serine biosynthesis (Figures 4C, 4D and S4B). The contribution of ^{13}C-glutamine-derived carbon to the serine and glycine pools of glucose-starved A549 cells increased exponentially over time and did not reach steady-state labeling over the 6h labeling period (Figures 4A-B). Indeed, the contribution of ^{13}C-glutamine-derived carbon to cellular serine and glycine pools reached 40% and 20%, respectively, when glucose-starved A549 cells were continuously labeled with ^{13}C-glutamine for 48h (Figure S4C and D).

Next we addressed whether PCK2 could regulate the production of ^{13}C-glutamine-derived serine and glycine in tumor cells. Silencing PCK2 in A549 cells ablated the ability of glucose-starved cells to produce serine (Figure 4E) and glycine (Figure 4F) from U-[^{13}C]-glutamine. ^{13}C-glutamine flux into the serine biosynthesis pathway was completely ablated in glucose-starved cells expressing *PCK2* shRNA (Figure S4E and F). Treatment of A549 cells with MPA also blocked glutamine-dependent production of serine (Figure 4G).

We hypothesized that PEP generated from OAA is exported from the mitochondria (Passarella et al., 2003; Satrustegui et al., 2007), converted by enolase to 3-PG, and then directed into the serine biosynthesis pathway by the activity of PHGDH (Figure 4H). To test this, we measured ^{13}C enrichment in serine (from U-[^{13}C]-glutamine tracer) in A549 cells with enolase or PHGDH expression silenced using siRNAs (Figure S4G). While levels of ^{13}C-labeled serine from U-[^{13}C]-glutamine increased significantly upon glucose deprivation in control cells, cells

transfected with siRNAs targeting *ENO1* or *PHGDH* displayed a marked reduction in glutamine-dependent serine biosynthesis (Figure S4H).

Glucose-derived serine and glycine contribute to the synthesis of purine nucleotides required for cell proliferation (Lunt and Vander Heiden, 2011). Thus, we investigated whether glutamine could substitute for glucose in supplying carbon for purine biosynthesis by measuring ^{13}C enrichment from U-[^{13}C]-glutamine in the purine nucleotide ATP. We detected a significant increase in the abundance of glutamine-derived ATP in cells grown under glucose-free conditions, which was blocked in cells treated with MPA (Figure 4I). An increased proportion of ATP (~12%) was labeled from U-[^{13}C]-glutamine, with the majority of the labeling at m+3 (Figure 4J).

PCK2 is required for glucose-independent cancer cell proliferation and tumor growth *in vivo*

Silencing *PCK2* by siRNA (Figure 5A) or shRNA (Figure S5B) blocked the ability of A549 and H1299 cells to proliferate in the absence of glucose. Consistent with the requirement of enolase and PHGDH to mediate glutamine-dependent serine biosynthesis (Figure S4H), knockdown of these enzymes also reduced the proliferation of A549 cells under glucose-free conditions (Figure 5B). Cell viability was unaffected by *PCK2*, *ENO1* or *PHGDH* knockdown regardless of glucose availability (Figure S5C).

To assess the impact of PCK2 on tumor growth *in vivo*, A549 and H1299 cells expressing either control or *PCK2*-specific shRNAs (Figures S5D and F) were injected into the flanks of nude mice, and tumor growth assessed over 65 days (Figures 5C and E). The majority of tumors expressing control shRNAs grew steadily

over time; however, tumors expressing *PCK2* shRNA failed to establish and grow substantially *in vivo* (Figures 5C and E). This was reflected in the reduced weight of *PCK2* shRNA-expressing tumors at the end of the experiment (Figures 5D and F). PCK2 protein expression was readily detected in end-stage control tumors, while suppression of PCK2 protein levels was maintained in tumors derived from cells expressing *PCK2* shRNA (Figures S5E and G).

The hypoxia inducible factors HIF-1α and EPAS1 regulate PCK2 expression under glucose limitation

We next examined the mechanisms of PCK2 regulation by glucose availability. Expression of both *PCK2* mRNA (Figure 6A) and protein (Figure 6B) was induced in NSCLC cells under conditions of glucose limitation. The activity of PCK2 is also dependent upon the production of mitochondrial GTP (mtGTP). mtGTP is generated by the SUCLG2 form of succinyl-CoA synthetase (SCS) in the TCA cycle (Stark et al., 2009). We found that the expression of the *SUCLG2* transcript (Figure 6C) and its metabolite product succinate (Figure S2A) were both elevated in glucose-starved A549 cells. Notably, the expression of *SUCLA2*, the ATP-generating form of SCS, was not affected by glucose availability (Figure 6C). Consistent with the requirement of SUCLG2 expression for PCK2 activity, silencing of *SUCLG2* (Figure S6A) led to a reduction in the glucose-independent proliferation of A549 cells (Figure 6D), similar to that observed when *PCK2* is silenced (Figure 5A). Silencing *SUCLA2* did not affect the glucose-independent proliferation of A549 cells (Figure 6D and S6A).

The hypoxia-inducible transcription factors HIF-1α and EPAS1/HIF-2α can promote PCK2 expression in K-ras mutant tumor cells (Chun et al., 2010). To test the role of HIF-1α and EPAS1 in glucose-dependent control of PCK2 expression in our

system, these genes were silenced in A549 cells (Figure S6B). Glucose-dependent stimulation of *PCK2* mRNA was not altered in A549 cells expressing HIF-1α siRNA, and only partially reduced upon EPAS1 knockdown (Figure S6C). However, silencing both HIF-1α and EPAS1 led to a ~25% reduction in *PCK2* mRNA expression. Similarly, silencing both HIF-1α and EPAS1 prevented the full induction of PCK2 protein by glucose withdrawal (Figure 6E).

Finally, we assessed the impact of HIF expression during glucose-independent proliferation. Knockdown of HIF-1α or EPAS1 alone had minimal effects on cell proliferation, while silencing both impaired the ability of A549 cells to proliferate under glucose-free conditions (Figure 6F).

PCK2 expression is deregulated in human cancer

We next investigated *PCK2* expression in human tumors through analysis of TCGA expression datasets for a variety of tumor types. *PCK2* mRNA expression was increased in a variety of tumor types (Figure 7A). The highest *PCK2* expression was found in thyroid, bladder, breast, kidney and NSCLC cancer tissue (Figure 7A). We next asked if elevated *PCK2* expression was observed in subsets of tumors within different tumor types. We considered the relative fraction of tumors with a z-score for *PCK2* >2 (illustrated by outlier dots on boxplots in Figure 7A, and summarized in the bottom panel). *PCK2* was overexpressed in 8.8% of lung squamous cell carcinoma (one of the major subtypes of NSCLC) samples from the TCGA datasets analyzed, which was the largest fraction among all tumor types examined.

We also assessed PCK2 protein levels in tumor samples isolated from human NSCLC patients. Examples of PCK2 protein expression in normal and tumor tissue from the lungs of 7 NSCLC patients are shown in Figure 7B, while Figure S7 presents

PCK2 protein levels in normal and tumor tissue from each of the 29 patients analyzed. Quantification of PCK2 protein expression in these primary human lung cancer samples revealed a significant increase in PCK2 protein levels in 15/29 (52%) of lung tumors (at $p<0.05$; Kruskal-Wallis test) when compared to patient-matched normal tissue (Figure 7C), compared to a decrease in PCK2 expression in only 10% of tumors (3/29, $p<0.05$). Together these data indicate that PCK2 expression is enriched in a number of tumor types, including NSCLC.

Discussion

Glucose is an important carbon source for proliferating cells, and is used to generate both ATP and precursors for macromolecular synthesis (Lunt and Vander Heiden, 2011). However, reduced glucose availability combined with the high demand for nutrients by cancer cells can lead to metabolic stress in tumors (Cantor and Sabatini, 2012; Jones and Thompson, 2009). Mounting evidence indicates that cancer cells and some non-malignant cells can engage glucose-independent metabolism to maintain cell proliferation and viability when glucose is limiting (Birsoy et al., 2014; Blagih et al., 2015; Glick et al., 2014; Le et al., 2012; Pasto et al., 2014). Tumor cells capable of using alternate substrates for biosynthetic and bioenergetic needs would gain a survival and proliferative advantage in microenvironments with limited resources. Using systems-level analysis combining both transcriptional and metabolic profiling data, we have identified the gluconeogenic enzyme PCK2 as a key regulator of tumor cell metabolic flexibility. We demonstrate here that PCK2 mediates a metabolic shunt in response to glucose deprivation, which supplies carbon from glutamine, rather than glucose, to generate glycolytic pathway intermediates required for biosynthesis and cell proliferation. Our data implicate PCK2-dependent metabolic reprogramming as a mechanism for glucose-independent tumor cell growth.

TCA cycle metabolism and OXPHOS are essential for maintaining energetic homeostasis in glucose-starved cells. This is achieved in part by glutamine-dependent pyruvate cycling through malic enzyme activity (Guay et al., 2007). Our data indicate that pyruvate cycling can also be mediated by PCK2 in glucose-starved tumor cells similar to that observed in pancreatic β-cells (Stark et al., 2009). However, silencing *PCK2* in glucose-starved A549 cells only modestly affected pyruvate cycling, suggesting alternate fates for PEP in tumor cells. We found that PCK2-dependent

production of PEP could also provide tumor cells growing in a low glucose environment with a supply of glycolytic intermediates needed to maintain cell proliferation.

Serine biosynthesis is a key metabolic pathway for cell proliferation, contributing carbon to many anabolic processes such as protein, glutathione, nucleotide, and phospholipid biosynthesis (Locasale, 2013; Vander Heiden et al., 2011). Under standard growth conditions, either exogenous serine or serine generated *de novo* from the glycolytic intermediate 3-phosphoglycerate (3-PG) can be used for anabolic growth (Chaneton et al., 2012; Labuschagne et al., 2014; Locasale et al., 2011). Here, we demonstrate that glutamine can substitute for glucose in serine and glycine biosynthesis in tumor cells with elevated PCK2 expression. Interestingly, despite the availability of exogenous serine and glycine, PHGDH was still required for tumor cell proliferation under low glucose conditions, suggesting that flux through this pathway contributes to cell growth even when the end products of the pathway are plentiful. *PHGDH* amplification is observed in some cancers (Locasale et al., 2011; Possemato et al., 2011), which may provide metabolic flexibility to tumors by fueling serine biosynthesis from multiple carbon sources.

Our results also indicate that glutamine can be used as a carbon source for nucleotide biosynthesis under conditions of glucose deprivation. Two carbons in purine nucleotides are derived from glycine and two one-carbon units are provided by *N*-^{10}-formyl-tetrahydrofolate, which acquires most of their carbon units from serine (Lunt and Vander Heiden, 2011). Thus, *de novo* serine biosynthesis could account for the ^{13}C-glutamine labeling patterns we observed in ATP. Another possibility is that ^{13}C-glutamine-derived glyceraldehyde 3-phosphate enters the non-oxidative arm of the pentose phosphate pathway to generate 5-phosphoribosyl-α-pyrophosphate

(PRPP) for nucleotide biosynthesis. It is unclear whether glutamine is sufficient to supply the glycolytic intermediates to generate nucleotide sugars, or whether these are sourced from other nutrients in glucose starved cells.

Increased glutamine/glutamate metabolism forms only one node of the metabolic adaptation network mediated by PCK2, suggesting that other substrates may feed into the network to help supply biosynthetic intermediates. Recent work suggests that PCK2 can mediate the conversion of lactate to PEP in lung cancer cells (Leithner et al., 2014), although this would require a supply of lactate from the tumor microenvironment as very little lactate is found in tumor cells experiencing glucose deprivation. Other anapleurotic substrates capable of generating OAA could function as substrates for PCK2-dependent PEP production under low glucose conditions, such as branched chain amino acids (BCAAs), which can enter the TCA cycle through metabolism of propionyl-CoA (Stark and Kibbey, 2014). Fructose-1,6-bisphosphatase, another enzyme involved in gluconeogenesis, can promote the viability of metastatic breast cancer cells by increasing glutamine and BCAA metabolism (Chen et al., 2015). Indeed, branched-chain amino acid transaminase 1 (BCAT1) is significantly upregulated in our metabolic network, as are the levels of several BCAAs (leucine, valine and isoleucine). β-oxidation of lipids may provide another carbon source for biosynthetic growth under glucose limitation (Vacanti et al., 2014).

PCK2 appears to be a glucose-regulated gene, as both mRNA and protein levels are significantly induced upon glucose withdrawal in tumor cells. PCK2 activity also depends on mitochondrial GTP (mtGTP), which is generated by the SUCLG2 form of succinyl-CoA synthetase (SCS) in the mitochondrial matrix (Stark et al., 2009). Expression of both *SUCLG2* and *PCK2* mRNA are stimulated by

glucose withdrawal, suggesting a coordinated effort to enhance PCK2 activity under low glucose conditions. Our data indicate that HIF-1α and EPAS1/HIF-2α act synergistically to induce PCK2 expression and facilitate proliferation under glucose-free conditions. While HIF-1α has been implicated in gluconeogenesis and regulation of PCK1 expression in the liver (Choi et al., 2005; Tajima et al., 2009), PCK1 was not abundantly expressed in NSCLC cells, nor was HIF-1α alone required for PCK2 expression, suggesting a more prominent role for EPAS1/HIF-2α in glucose-dependent control of PCK2. Thus, while HIFs play prominent roles in metabolic regulation during hypoxia (Mucaj et al., 2012), HIF-dependent re-wiring of the TCA cycle through PCK2 helps provide tumor cells with additional metabolic flexibility for glucose-independent cell growth.

To date, there has been little focus on PEPCK in the context of cancer. Here we have presented evidence for PCK2-mediated metabolic adaptation in tumor cells and elevated PCK2 expression in human tumor subsets including NSCLC. We hypothesize that PCK2 could provide a selective growth advantage to tumor cells growing in nutrient-poor environments, enabling them to use PEP, supplied by glutamine or other anapleurotic substrates, to support TCA cycle metabolism and glycolytic intermediates for biosynthesis. In this light, targeting PCK2-mediated metabolic adaptation may be an effective strategy for certain cancer subtypes, particularly NSCLC.

Experimental Procedures

Cell culture

A549 and H1299 cell lines were obtained from ATCC (Manassas, VA, USA). Cells were cultured in 'growth medium' (DMEM (A549 cells) or RPMI (H1299 cells)) supplemented with 10% fetal bovine serum (FBS), penicillin, streptomycin, glutamine, and non-essential amino acids (for H1299 cells). For glucose limitation experiments, cells were cultured in glucose- and glutamine-free DMEM supplemented with 10% dialysed FBS (Wisent, Saint-John-Baptiste, QC, Canada) and glutamine (2 mM) and glucose (25 mM) added as required. *PCK2* knockdown was achieved using lentiviral shRNA vectors from the TRC shRNA collection (ID numbers listed in Supplementary Information). Lentiviral supernatants were generated as described (Huang et al., 2012). Transient knockdown of PCK2, ENO1, PHGDH, HIF1A, EPAS1, SUCLG2 and SUCLA2 was achieved using the SMARTpool ON-TARGETplus siRNA reagent (composed of 4 individual siRNAs for each target) from GE Dharmacon (Layette, CO, USA). The PEPCK inhibitor 3-mercaptopicolinic acid (MPA) was obtained from Santa Cruz Biotechnology (Dallas, TX, USA).

Cell proliferation and viability assays

Cells were seeded in 384 well plates (500 cells/well) in growth medium as previously described (Vincent et al., 2015). After 24h, growth medium was replaced with fresh medium containing 25 or 0 mM glucose. Cells were fixed with 4% formaldehyde, stained with Hoechst DNA stain, and cell number determined by nuclei counting. Images were taken using an Operetta High Content Imaging System and analyzed using Harmony High Content Imaging and Analysis Software (Perkin Elmer, Waltham, MA, USA). Cell viability was determined by viability dye exclusion by

flow cytometry using propidium iodide (PI). Cells were analyzed using a Gallios flow cytometer (Beckman Coulter, Fullerton, CA) and data analyzed using FlowJo software (TreeStar).

Metabolite Profiling by GC- and LC-MS

Cellular metabolites were extracted and analyzed either by GC-MS or LC-MS using previously described protocols (Dupuy et al., 2013; Faubert et al., 2014; McGuirk et al., 2013). For GC-MS, metabolite extracts were derivatized using N-(*tert*-butyldimethylsilyl)-N-methyltrifluoroacetamide (MTBSTFA) as previously described (Faubert et al., 2013). D-myristic acid (750 ng/sample) was added as an internal standard to metabolite extracts, and metabolite abundance was expressed relative to the internal standard and normalized to cell number. Liquid chromatography was performed using a 1290 Infinity ultra-performance LC system (Agilent Technologies, Santa Clara, CA, USA) equipped with a Scherzo 3 μm, 3.0×150mm SM-C18 column (Imtakt Corp, Japan). LC-MS analysis was performed on an Agilent 6540 UHD Accurate-Mass Q-TOF mass spectrometer (Agilent Technologies, Santa Clara, CA, USA). For SITA experiments, cells were cultured with U-[^{13}C]-glutamine (Cambridge Isotopes) for the times indicated. Mass isotopomer distribution was determined using a custom algorithm developed at McGill University (McGuirk et al., 2013).

RNA-Seq analysis and Network-based Data Integration

For RNA-seq experiments, A549 cells were cultured in the presence or absence of glucose (25 mM) for 48 hours prior to RNA extraction. cDNA synthesis and library construction was conducted as previously described (Jha et al., 2015). Libraries were sequenced using a HiSeq 2500 (Illumina) using 50bpX25bp pair-end sequencing.

To construct the integrated metabolic network illustrated in Figure 1, A549 cells were cultured in medium containing 25 or 0 mM glucose for 48 hours prior to either RNA or metabolite extraction and analysis. Integration of metabolite and RNA expression datasets was conducted as previously described (Jha et al., 2015). Additional details are provided in Supplementary Information.

Immunoblotting and Quantitative Real-Time PCR

Lysates of NSCLC cell lines or tissue were subjected to SDS-PAGE and western blotting as previously described (Vincent et al., 2011). Primary antibodies to PCK2 and actin, as well as HRP-conjugated anti-rabbit and anti-mouse secondary antibodies were obtained from Cell Signaling Technology (Danvers, MA, USA). All human NSCLC tissue lysate immunoblots were incubated with fluorescently labeled anti-rabbit or anti-mouse secondary antibodies and analyzed and quantified using an Odyssey® Sa Infrared Imaging System (Licor, Lincoln, NE, USA). Quantitative PCR was performed as previously described (Faubert et al., 2013). Primer sequences have previously been described (Faubert et al., 2013) or are listed in Table S1.

Tumor xenograft assays

A549 and H1299 cells expressing either control or shRNA targeting *PCK2* were counted (2 million cells/injection) and resuspended in 50% matrigel/50% PBS (200µl/injection) and injected subcutaneously into the flanks of nude mice (Charles River, Seattle, WA, USA). Tumor length (l) and width (w) was measured every 3-4 days with calipers and the tumor volume (V) was calculated ($V=1/2(l x w^2)$). After 65 days the mice were sacrificed and the tumors were dissected out and weighed.

TCGA data analysis

TCGA data for 35 tumor studies that contained mRNA expression data was accessed using the R-interface cgdsr to cBio Cancer Genomics Portal (Cerami et al., 2012; Gao et al., 2013). For each dataset, *PCK2* expression relative to *ACTB* was determined for each patient sample. Nine studies with different tissues from the whole spectrum of relative *PCK2* expression were analyzed.

NSCLC patients and tissue samples

Collection of samples, details of the cohort and sample extraction have been previously described (Vincent et al., 2014; Vincent et al., 2011). Briefly, three distinct samples of lung tumour tissue and adjacent normal lung from the resection margin were taken, flash frozen in liquid nitrogen, and stored at –80°C until further analysis. Only those NSCLC tumour samples comprising at least 90% tumour tissue were analyzed. Tissues were homogenized in 1% NP40 lysis buffer using a Polytron homogenizer to generate tissue lysates for SDS-PAGE analysis.

Statistical Analysis

Statistics were determined using paired Student's t-test using Prism software (GraphPad, San Diego, CA, USA) unless otherwise stated. Data are calculated as the mean ± SEM for biological triplicates unless otherwise stated. Statistical significance is represented in figures by: *, $p<0.05$; **, $p<0.01$; ***, $p<0.001$; ****, $p<0.0001$.

Acknowledgements

We acknowledge M Hetzel, J Pawade, M Sohail and L Phillips for the collection of NSCLC tissue. W Reintsch gave technical assistance and S Huang provided access to the shRNAs. The work was supported by grants from the McGill Integrated Cancer Research Training Program (to EEV, PPC and BRF), the Government of Russian Federation (to AS, 074-U01), Fonds de recherche Santé Québec (TG), Wellcome Trust Seeding Drug Discovery Award (to JMT) and CIHR (MOP-93799), Terry Fox Foundation, and Cancer Research Society (to RGJ).

Accession Numbers

Raw and processed sequencing data are deposited at Pubmed GEO under GSE66556.

References

Ahn, C.S., and Metallo, C.M. (2015). Mitochondria as biosynthetic factories for cancer proliferation. Cancer & metabolism *3*, 1.

Birsoy, K., Possemato, R., Lorbeer, F.K., Bayraktar, E.C., Thiru, P., Yucel, B., Wang, T., Chen, W.W., Clish, C.B., and Sabatini, D.M. (2014). Metabolic determinants of cancer cell sensitivity to glucose limitation and biguanides. Nature *508*, 108-112.

Blagih, J., Coulombe, F., Vincent, E.E., Dupuy, F., Galicia-Vazquez, G., Yurchenko, E., Raissi, T.C., van der Windt, G.J., Viollet, B., Pearce, E.L.*, et al.* (2015). The Energy Sensor AMPK Regulates T Cell Metabolic Adaptation and Effector Responses In Vivo. Immunity *42*, 41-54.

Cantor, J.R., and Sabatini, D.M. (2012). Cancer cell metabolism: one hallmark, many faces. Cancer discovery *2*, 881-898.

Cerami, E., Gao, J., Dogrusoz, U., Gross, B.E., Sumer, S.O., Aksoy, B.A., Jacobsen, A., Byrne, C.J., Heuer, M.L., Larsson, E.*, et al.* (2012). The cBio cancer genomics portal: an open platform for exploring multidimensional cancer genomics data. Cancer discovery *2*, 401-404.

Chaneton, B., Hillmann, P., Zheng, L., Martin, A.C., Maddocks, O.D., Chokkathukalam, A., Coyle, J.E., Jankevics, A., Holding, F.P., Vousden, K.H.*, et al.* (2012). Serine is a natural ligand and allosteric activator of pyruvate kinase M2. Nature *491*, 458-462.

Chen, J., Lee, H.J., Wu, X., Huo, L., Kim, S.J., Xu, L., Wang, Y., He, J., Bollu, L.R., Gao, G.*, et al.* (2015). Gain of glucose-independent growth upon metastasis of breast cancer cells to the brain. Cancer Res *75*, 554-565.

Choi, J.H., Park, M.J., Kim, K.W., Choi, Y.H., Park, S.H., An, W.G., Yang, U.S., and Cheong, J. (2005). Molecular mechanism of hypoxia-mediated hepatic gluconeogenesis by transcriptional regulation. FEBS Lett *579*, 2795-2801.

Chun, S.Y., Johnson, C., Washburn, J.G., Cruz-Correa, M.R., Dang, D.T., and Dang, L.H. (2010). Oncogenic KRAS modulates mitochondrial metabolism in human colon cancer cells by inducing HIF-1alpha and HIF-2alpha target genes. Molecular cancer *9*, 293.

DeBerardinis, R.J., Lum, J.J., Hatzivassiliou, G., and Thompson, C.B. (2008a). The biology of cancer: metabolic reprogramming fuels cell growth and proliferation. Cell Metab *7*, 11-20.

DeBerardinis, R.J., Mancuso, A., Daikhin, E., Nissim, I., Yudkoff, M., Wehrli, S., and Thompson, C.B. (2007). Beyond aerobic glycolysis: transformed cells can engage in glutamine metabolism that exceeds the requirement for protein and nucleotide synthesis. Proc Natl Acad Sci U S A *104*, 19345-19350.

Deberardinis, R.J., Sayed, N., Ditsworth, D., and Thompson, C.B. (2008b). Brick by brick: metabolism and tumor cell growth. Curr Opin Genet Dev *18*, 54-61.

Dupuy, F., Griss, T., Blagih, J., Bridon, G., Avizonis, D., Ling, C., Dong, Z., Siwak, D.R., Annis, M.G., Mills, G.B.*, et al.* (2013). LKB1 is a central regulator of tumor initiation and pro-growth metabolism in ErbB2-mediated breast cancer. Cancer & metabolism *1*, 18.

Faubert, B., Boily, G., Izreig, S., Griss, T., Samborska, B., Dong, Z., Dupuy, F., Chambers, C., Fuerth, B.J., Viollet, B.*, et al.* (2013). AMPK Is a Negative Regulator

of the Warburg Effect and Suppresses Tumor Growth In Vivo. Cell Metab *17*, 113-124.

Faubert, B., Vincent, E.E., Griss, T., Samborska, B., Izreig, S., Svensson, R.U., Mamer, O.A., Avizonis, D., Shackelford, D.B., Shaw, R.J.*, et al.* (2014). Loss of the tumor suppressor LKB1 promotes metabolic reprogramming of cancer cells via HIF-1alpha. Proc Natl Acad Sci U S A *111*, 2554-2559.

Gao, J., Aksoy, B.A., Dogrusoz, U., Dresdner, G., Gross, B., Sumer, S.O., Sun, Y., Jacobsen, A., Sinha, R., Larsson, E.*, et al.* (2013). Integrative analysis of complex cancer genomics and clinical profiles using the cBioPortal. Sci Signal *6*, pl1.

Glick, G.D., Rossignol, R., Lyssiotis, C.A., Wahl, D., Lesch, C., Sanchez, B., Liu, X., Hao, L.Y., Taylor, C., Hurd, A.*, et al.* (2014). Anaplerotic metabolism of alloreactive T cells provides a metabolic approach to treat graft-versus-host disease. J Pharmacol Exp Ther *351*, 298-307.

Guay, C., Madiraju, S.R., Aumais, A., Joly, E., and Prentki, M. (2007). A role for ATP-citrate lyase, malic enzyme, and pyruvate/citrate cycling in glucose-induced insulin secretion. J Biol Chem *282*, 35657-35665.

Hirayama, A., Kami, K., Sugimoto, M., Sugawara, M., Toki, N., Onozuka, H., Kinoshita, T., Saito, N., Ochiai, A., Tomita, M.*, et al.* (2009). Quantitative metabolome profiling of colon and stomach cancer microenvironment by capillary electrophoresis time-of-flight mass spectrometry. Cancer Res *69*, 4918-4925.

Huang, S., Holzel, M., Knijnenburg, T., Schlicker, A., Roepman, P., McDermott, U., Garnett, M., Grernrum, W., Sun, C., Prahallad, A.*, et al.* (2012). MED12 controls the

response to multiple cancer drugs through regulation of TGF-beta receptor signaling. Cell *151*, 937-950.

Jha, A.K., Huang, S.C.-C., Sergushichev, A., Lampropoulou, V., Ivanova, Y., Loginicheva, E., Chmielewski, K., Stewart, K.M., Ashall, J., Everts, B.*, et al.* (2015). Network integration of parallel metabolomic-transcriptional data reveals novel metabolic modules regulating divergent macrophage polarization. Immunity *42*, 419-430.

Jones, R.G., and Thompson, C.B. (2009). Tumor suppressors and cell metabolism: a recipe for cancer growth. Genes Dev *23*, 537-548.

Labuschagne, C.F., van den Broek, N.J., Mackay, G.M., Vousden, K.H., and Maddocks, O.D. (2014). Serine, but not glycine, supports one-carbon metabolism and proliferation of cancer cells. Cell reports *7*, 1248-1258.

Le, A., Lane, A.N., Hamaker, M., Bose, S., Gouw, A., Barbi, J., Tsukamoto, T., Rojas, C.J., Slusher, B.S., Zhang, H.*, et al.* (2012). Glucose-independent glutamine metabolism via TCA cycling for proliferation and survival in B cells. Cell Metab *15*, 110-121.

Leithner, K., Hrzenjak, A., Trotzmuller, M., Moustafa, T., Kofeler, H.C., Wohlkoenig, C., Stacher, E., Lindenmann, J., Harris, A.L., Olschewski, A.*, et al.* (2014). PCK2 activation mediates an adaptive response to glucose depletion in lung cancer. Oncogene.

Locasale, J.W. (2013). Serine, glycine and one-carbon units: cancer metabolism in full circle. Nat Rev Cancer *13*, 572-583.

Locasale, J.W., Grassian, A.R., Melman, T., Lyssiotis, C.A., Mattaini, K.R., Bass, A.J., Heffron, G., Metallo, C.M., Muranen, T., Sharfi, H., *et al.* (2011). Phosphoglycerate dehydrogenase diverts glycolytic flux and contributes to oncogenesis. Nature genetics *43*, 869-874.

Lunt, S.Y., and Vander Heiden, M.G. (2011). Aerobic glycolysis: meeting the metabolic requirements of cell proliferation. Annual review of cell and developmental biology *27*, 441-464.

McGuirk, S., Gravel, S.P., Deblois, G., Papadopoli, D.J., Faubert, B., Wegner, A., Hiller, K., Avizonis, D., Akavia, U.D., Jones, R.G., *et al.* (2013). PGC-1alpha supports glutamine metabolism in breast cancer. Cancer & metabolism *1*, 22.

Metallo, C.M., Gameiro, P.A., Bell, E.L., Mattaini, K.R., Yang, J., Hiller, K., Jewell, C.M., Johnson, Z.R., Irvine, D.J., Guarente, L., *et al.* (2012). Reductive glutamine metabolism by IDH1 mediates lipogenesis under hypoxia. Nature *481*, 380-384.

Mucaj, V., Shay, J.E., and Simon, M.C. (2012). Effects of hypoxia and HIFs on cancer metabolism. International journal of hematology *95*, 464-470.

Mullen, A.R., Wheaton, W.W., Jin, E.S., Chen, P.H., Sullivan, L.B., Cheng, T., Yang, Y., Linehan, W.M., Chandel, N.S., and DeBerardinis, R.J. (2012). Reductive carboxylation supports growth in tumour cells with defective mitochondria. Nature *481*, 385-388.

Passarella, S., Atlante, A., Valenti, D., and de Bari, L. (2003). The role of mitochondrial transport in energy metabolism. Mitochondrion *2*, 319-343.

Pasto, A., Bellio, C., Pilotto, G., Ciminale, V., Silic-Benussi, M., Guzzo, G., Rasola, A., Frasson, C., Nardo, G., Zulato, E.*, et al.* (2014). Cancer stem cells from epithelial ovarian cancer patients privilege oxidative phosphorylation, and resist glucose deprivation. Oncotarget *5*, 4305-4319.

Possemato, R., Marks, K.M., Shaul, Y.D., Pacold, M.E., Kim, D., Birsoy, K., Sethumadhavan, S., Woo, H.K., Jang, H.G., Jha, A.K.*, et al.* (2011). Functional genomics reveal that the serine synthesis pathway is essential in breast cancer. Nature *476*, 346-350.

Satrustegui, J., Pardo, B., and Del Arco, A. (2007). Mitochondrial transporters as novel targets for intracellular calcium signaling. Physiological reviews *87*, 29-67.

Stark, R., and Kibbey, R.G. (2014). The mitochondrial isoform of phosphoenolpyruvate carboxykinase (PEPCK-M) and glucose homeostasis: has it been overlooked? Biochim Biophys Acta *1840*, 1313-1330.

Stark, R., Pasquel, F., Turcu, A., Pongratz, R.L., Roden, M., Cline, G.W., Shulman, G.I., and Kibbey, R.G. (2009). Phosphoenolpyruvate cycling via mitochondrial phosphoenolpyruvate carboxykinase links anaplerosis and mitochondrial GTP with insulin secretion. J Biol Chem *284*, 26578-26590.

Tajima, T., Goda, N., Fujiki, N., Hishiki, T., Nishiyama, Y., Senoo-Matsuda, N., Shimazu, M., Soga, T., Yoshimura, Y., Johnson, R.S.*, et al.* (2009). HIF-1alpha is necessary to support gluconeogenesis during liver regeneration. Biochem Biophys Res Commun *387*, 789-794.

Urbina, J.A., Osorno, C.E., and Rojas, A. (1990). Inhibition of phosphoenolpyruvate carboxykinase from Trypanosoma (Schizotrypanum) cruzi epimastigotes by 3-

mercaptopicolinic acid: in vitro and in vivo studies. Archives of biochemistry and biophysics *282*, 91-99.

Vacanti, N.M., Divakaruni, A.S., Green, C.R., Parker, S.J., Henry, R.R., Ciaraldi, T.P., Murphy, A.N., and Metallo, C.M. (2014). Regulation of substrate utilization by the mitochondrial pyruvate carrier. Mol Cell *56*, 425-435.

Vander Heiden, M.G., Lunt, S.Y., Dayton, T.L., Fiske, B.P., Israelsen, W.J., Mattaini, K.R., Vokes, N.I., Stephanopoulos, G., Cantley, L.C., Metallo, C.M.*, et al.* (2011). Metabolic pathway alterations that support cell proliferation. Cold Spring Harb Symp Quant Biol *76*, 325-334.

Vincent, E.E., Coelho, P.P., Blagih, J., Griss, T., Viollet, B., and Jones, R.G. (2015). Differential effects of AMPK agonists on cell growth and metabolism. Oncogene. *34*, 3627-39.

Vincent, E.E., Elder, D.J., O'Flaherty, L., Pardo, O.E., Dzien, P., Phillips, L., Morgan, C., Pawade, J., May, M.T., Sohail, M.*, et al.* (2014). Glycogen synthase kinase 3 protein kinase activity is frequently elevated in human non-small cell lung carcinoma and supports tumour cell proliferation. PLoS One *9*, e114725.

Vincent, E.E., Elder, D.J., Phillips, L., Heesom, K.J., Pawade, J., Luckett, M., Sohail, M., May, M.T., Hetzel, M.R., and Tavare, J.M. (2011). Overexpression of the TXNDC5 protein in non-small cell lung carcinoma. Anticancer Res *31*, 1577-1582.

Wise, D.R., Ward, P.S., Shay, J.E., Cross, J.R., Gruber, J.J., Sachdeva, U.M., Platt, J.M., DeMatteo, R.G., Simon, M.C., and Thompson, C.B. (2011). Hypoxia promotes isocitrate dehydrogenase-dependent carboxylation of alpha-ketoglutarate to citrate to support cell growth and viability. Proc Natl Acad Sci U S A *108*, 19611-19616.

Yang, C., Ko, B., Hensley, C.T., Jiang, L., Wasti, A.T., Kim, J., Sudderth, J., Calvaruso, M.A., Lumata, L., Mitsche, M.*, et al.* (2014). Glutamine oxidation maintains the TCA cycle and cell survival during impaired mitochondrial pyruvate transport. Mol Cell *56*, 414-424.

Yang, C., Sudderth, J., Dang, T., Bachoo, R.G., McDonald, J.G., and DeBerardinis, R.J. (2009). Glioblastoma cells require glutamate dehydrogenase to survive impairments of glucose metabolism or Akt signaling. Cancer Res *69*, 7986-7993.

Figure Legends

Figure 1. Network-based data integration reveals distinct metabolic nodes in tumor cells adapted to glucose-independent proliferation.

(A) Proliferation of A549 and H1299 cells over 96h in either nutrient replete medium (+Glc, +Q), medium without glucose (-Glc, +Q) or medium without glutamine (+Glc, -Q). Data are represented as mean +/- SEM for biological replicates (n=5).

(B) Metabolite set enrichment analysis for differentially regulated metabolic pathways induced upon glucose deprivation. A549 cells were cultured in the presence (Glc+) or absence (Glc-) of glucose for 48h before metabolite abundances were determined by GC and LC-MS (full metabolite profile in Figure S1).

(C) Integrated metabolic network analysis for A549 cells cultured in the presence (Glc+) or absence (Glc-) of glucose for 48h. The direction and magnitude of the fold-change in enzyme expression or metabolite abundance between conditions is indicated on a red (enriched in Glc-) to green (enriched in Glc+) color scale. Enzymes are represented by edges (connecting lines between metabolites) with the color of the edge indicating fold-change and the thickness reflecting the significance of differential expression. Round nodes represent metabolites, with the differential abundance of each metabolite indicated by the size of the node. Major features of glucose deprivation identified by the network analysis are highlighted by bold titles and background shading.

Figure 2. Glucose withdrawal redirects glutamine metabolism to maintain the TCA cycle and for the production of PEP.

(A) Model of glutamine dependent anapleurosis in the TCA cycle. U-[^{13}C]-Q fuels TCA cycle anaplerosis through α-KG to OAA via succinate, fumarate and malate.

Oxidative metabolism of glutamine yields citrate m+4, while reductive carboxylation of glutamine results in citrate m+5. Abbreviations: Glc, glucose; Gln, glutamine; Ac-CoA, acety-CoA; α-KG, α-ketoglutarate; OAA, oxaloacetate.

(B) Proportion of glutamate and α-KG containing five ^{13}C carbons (m+5) and the proportion of succinate, fumarate, malate and aspartate containing four ^{13}C carbons (m+4) in A549 cells cultured for 12h in the presence (+) or absence (-) of unlabeled glucose (Glc). Cells were cultured with U-[^{13}C]-Q for the last 6h.

(C) Mass isotopologues of the citrate pool in A549 cells, cultured as in (B).

(D) Contribution of the mass isotopologues of citrate (m+4, m+5 and m+6) to the total citrate pool in A549 cells. Cells were pre-incubated in the presence or absence of glucose for 6h before incubation with U-[^{13}C]-Q (time 0). Cells extracts were harvested at the time points shown.

(E-F) Glutamine contribution to pyruvate and PEP in glucose starved A549 cells. (E) Top: Relative abundance and contribution of U-[^{13}C]-Q to pyruvate in A549 cells cultured as in (B). Bottom: Proportion of the pyruvate pool labeled by U-[^{13}C]-Q over time in A549 cells cultured as in (D).

(F) Relative abundance and proportion of the PEP pool labeled from U-[^{13}C]-Q over time in A549 cells cultured as in (E).

(G) Proportion of the m+6 mass isotopologue of citrate (top) and relative abundance of U-[^{13}C]-Q incorporated into pyruvate (middle) and PEP (bottom) in H1299 cells cultured as in (B).

(B-G) Data are represented as mean +/- SEM of three independent cultures.

See also Figure S2.

Figure 3. PEP production from glutamine in glucose-starved cells is dependent on PCK2.

(A) Immunoblot for PCK2 and actin on lysates from A549 and H1299 cells expressing control or *PCK2* shRNA. *PCK1*(1) and *PCK2*(2) represent two different shRNAs targeting *PCK2*.

(B) Schematic for proposed PCK2-mediated pyruvate cycling. Fully labeled OAA (m+4) is made from U-[^{13}C]-Q. PCK2 activity produces fully labeled PEP (m+3) from OAA. Pyruvate can be made using PEP through the activity of pyruvate kinase and this can re-enter the TCA cycle as acetyl-CoA.

(C) Relative abundance of U-[^{13}C]-Q incorporation into PEP in A549 and H1299 cells expressing control or *PCK2* shRNAs or upon treatment with the PEPCK inhibitor, MPA. Cells were cultured in the presence or absence of glucose for 12h, with U-[^{13}C]-Q added for the last 6h of incubation. Far right panel: A549 cells were treated with either DMSO (vehicle) or MPA throughout the 12h incubation.

(D) Relative abundance of U-[^{13}C]-Q incorporation into pyruvate in A549 and H1299 cells expressing control or *PCK2* shRNA or upon treatment with the PCK2 inhibitor, MPA. Cells were incubated as in (C).

(C-D) Data are represented as mean +/- SEM of three independent cultures.

See also Figure S3.

Figure 4. Serine, glycine and ATP are made from glutamine upon glucose withdrawal in a PCK2-dependent manner.

(A-D) U-[^{13}C]-Q incorporation into serine and glycine in glucose starved cells. A549 (A and B) or H1299 (C and D) cells were cultured for 12h in the presence or absence of glucose, followed by culture with U-[^{13}C]-Q for the last 6h of the 12h incubation.

Shown is the proportion of the serine (A) or glycine (B) pools labeled by U-[^{13}C]-Q in A549 cells over time. Levels of U-[^{13}C]-Q-derived serine (C) and glycine (D) in glucose-starved H1299 cells is shown.

(E-G) Relative abundance of U-[^{13}C]-Q incorporation into serine (E and G) and glycine (F) in A549 cells expressing control and *PCK2* shRNA (E and F) or upon treatment with MPA (G). Cells were cultured in the presence or absence of glucose for 12h, then cultured with U-[^{13}C]-Q for the last 6h of the 12h incubation. (G) A549 cells were treated with either DMSO (vehicle) or MPA throughout the 12h incubation.

(H) Schematic of PCK2-mediated labeling of serine for OAA. Fully labeled OAA (m+4) is made from U-[^{13}C]-Q. PCK2 activity produces fully labeled PEP (m+3) from OAA. Serine and glycine can be made using PEP through the activities of enolase and PHGDH. Abbreviations: 3-PG, 3-phosphoglycerate; Eno, enolase; PHGDH, phophoglycerate dehydrogenase.

(I) Abundance of ^{13}C-ATP in A549 cells cultured with U-[^{13}C]-Q for 48h in the presence or absence of glucose. Cells were treated with either DMSO (vehicle) or MPA throughout the 48h incubation.

(J) Mass isotopologues of the ATP pool in A549 cells cultured as in (I).

(A-G and I-J) Data are represented as mean +/- SEM of three independent cultures.

See also Figure S4.

Figure 5. Cancer cells require PCK2 to maintain glucose-independent proliferation and tumor growth *in vivo*.

(A) Proliferation of A549 and H1299 cells in glucose-free media over 96h following transfection with control or *PCK2* siRNA.

(B) Proliferation of A549 cells in glucose free media over 96h following transfection with the indicated siRNAs.

Each data point in A and B represents the average cell number of 5 wells in a 384 well plate.

(C-F) A549 and H1299 cells were injected into the flanks of nude mice. Growth of tumors derived from A549 cells expressing either control (n=6) or shRNA targeting *PCK2* (n=7) (C) and from H1299 cells expressing either control (n=7) or shRNA targeting *PCK2* (n=7) (D) is shown over 65 days. Tumor weights at the end of the experiment are also shown for A549 (D) and H1299 (F) cells. Data are represented as mean +/- SEM.

See also Figure S5.

Figure 6. PCK2 expression is regulated by glucose availability.

(A) Relative expression of *PCK2* mRNA as determined by qPCR. A549 cells were cultured in the presence or absence of glucose for up to 48h. Transcript levels were determined relative to *ACTB* mRNA levels, and normalized relative to expression at time 0. Data are represented as mean +/- SEM.

(B) Immunoblot for PCK2 and actin on lysates from A549 and H1299 cells incubated in the presence or absence of glucose for 48h.

(C) Relative expression of mRNA as measured by RNA-seq in A549 cells cultured in the presence or absence of glucose for 48h. Data were expressed relative to *SUCLG2* expression in cells grown under full glucose. Data are the mean +/- SEM of three independent cultures.

(D) Proliferation of A549 cells in glucose free media over 96h following transfection with indicated siRNAs. Each data point represents the average cell number of 5 wells in a 384 well plate (mean +/- SEM).

(E) Immunoblot for PCK2 and actin on lysates from A549 cells transfected with indicated siRNAs, then treated with or without glucose for 48h.

(F) Growth of A549 cells in glucose-free medium over 96 hours. A549 cells were transfected with indicated siRNAs prior to seeding for growth assay. Each data point represents the average cell number of 5 wells in a 384 well plate (mean +/- SEM).

See also Figure S6.

Figure 7. PCK2 expression is increased in human cancer.

(A) Boxplot of distribution of *PCK2* mRNA expression levels relative to *ACTB* in TCGA cancer studies. Studies were selected to represent whole spectrum of expression levels. The boxplot was cropped at the relative expression value of 0.05.

(B) Immunoblot for PCK2 on 3 individual samples of normal and tumor tissue samples from NSCLC patients. F_1-ATPase was used as a control for protein loading.

(C) Quantification of immunoblots for PCK2 expression from patient-matched normal and tumour tissues. Patients (n=29) are ranked based on percent change in PCK2 expression in tumour samples relative to patient-matched normal tissue. Statistical significance was determined by a Kruskal-Wallis test, * $p<0.05$.

See also Figure S7.

Vincent_Fig1

A

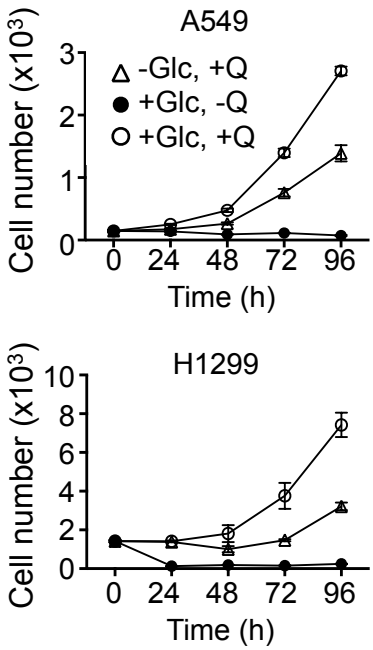

B

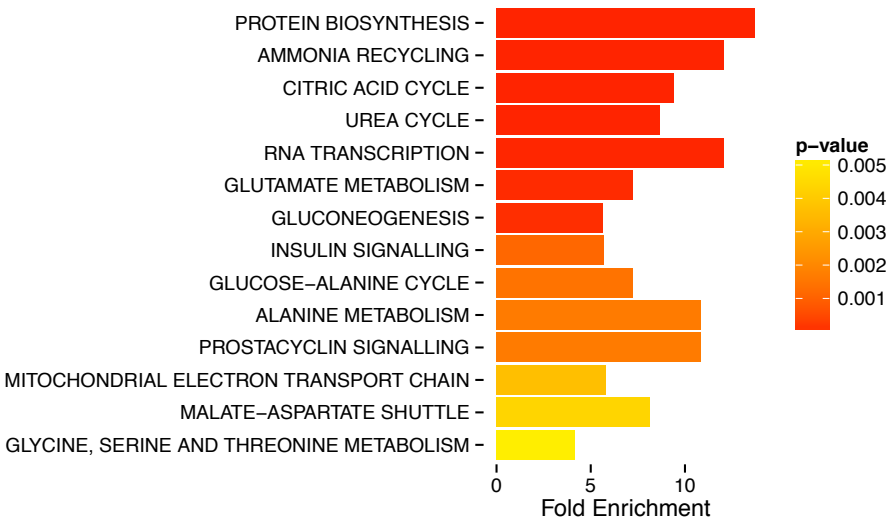

C

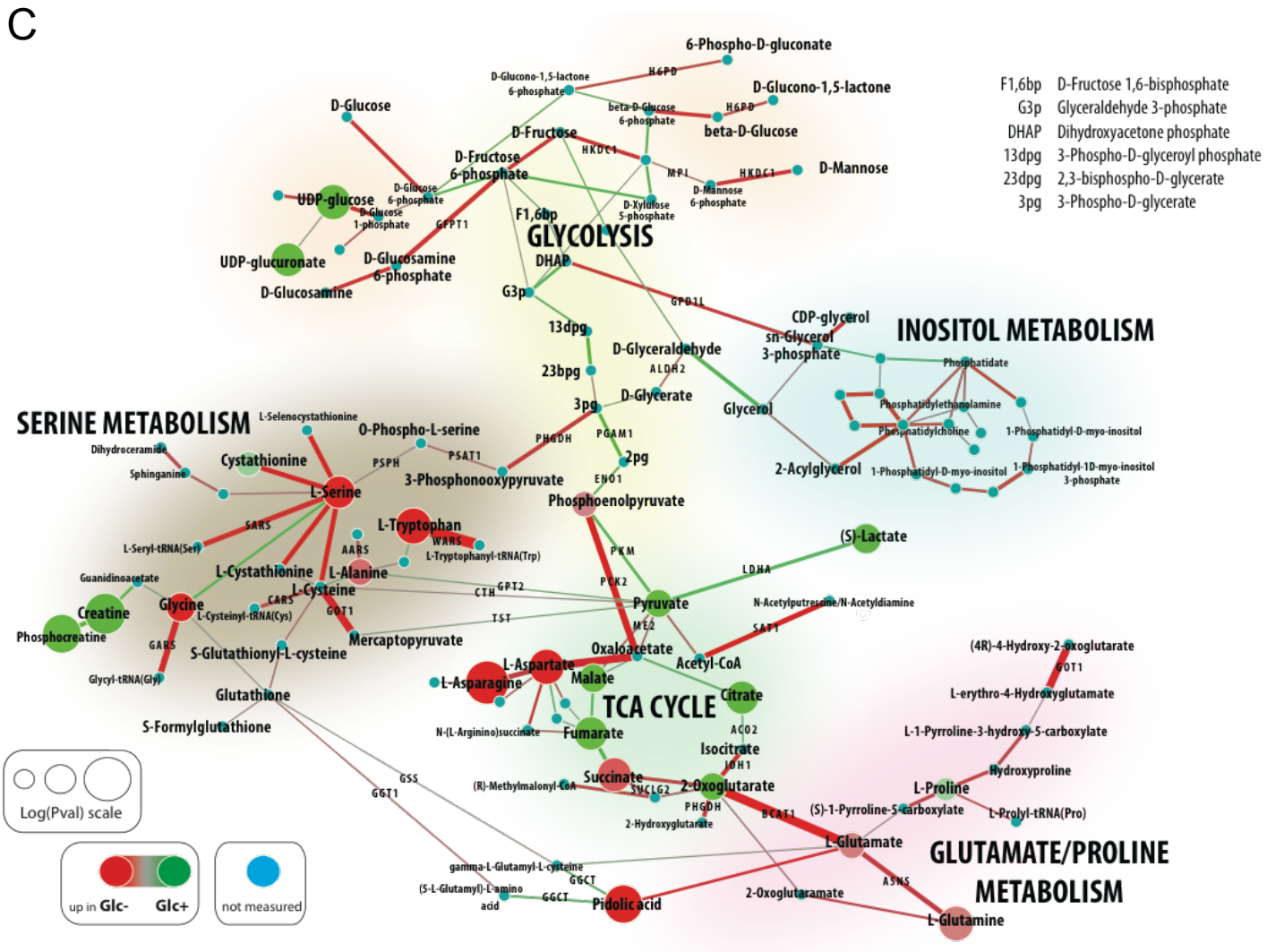

Vincent_Fig2

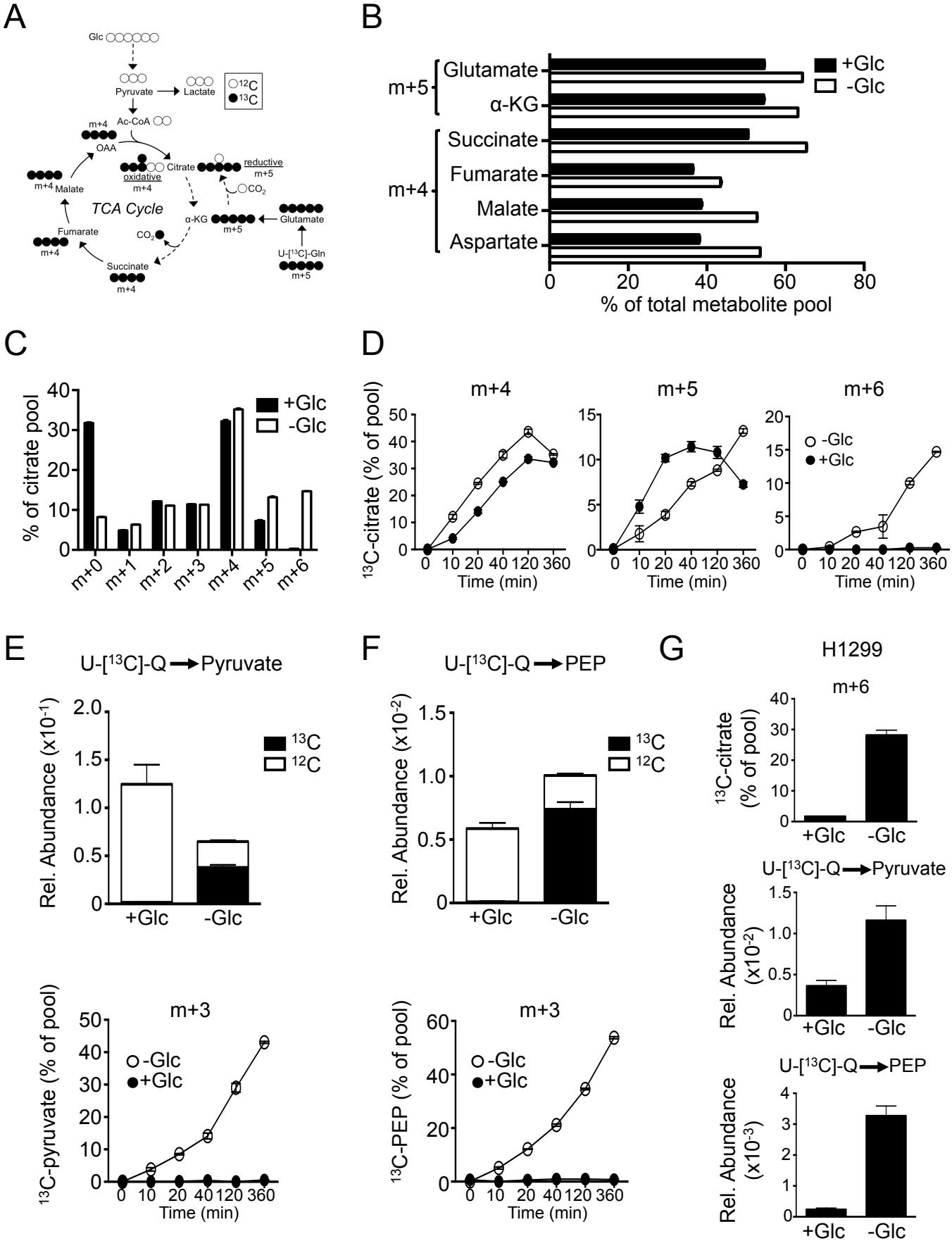

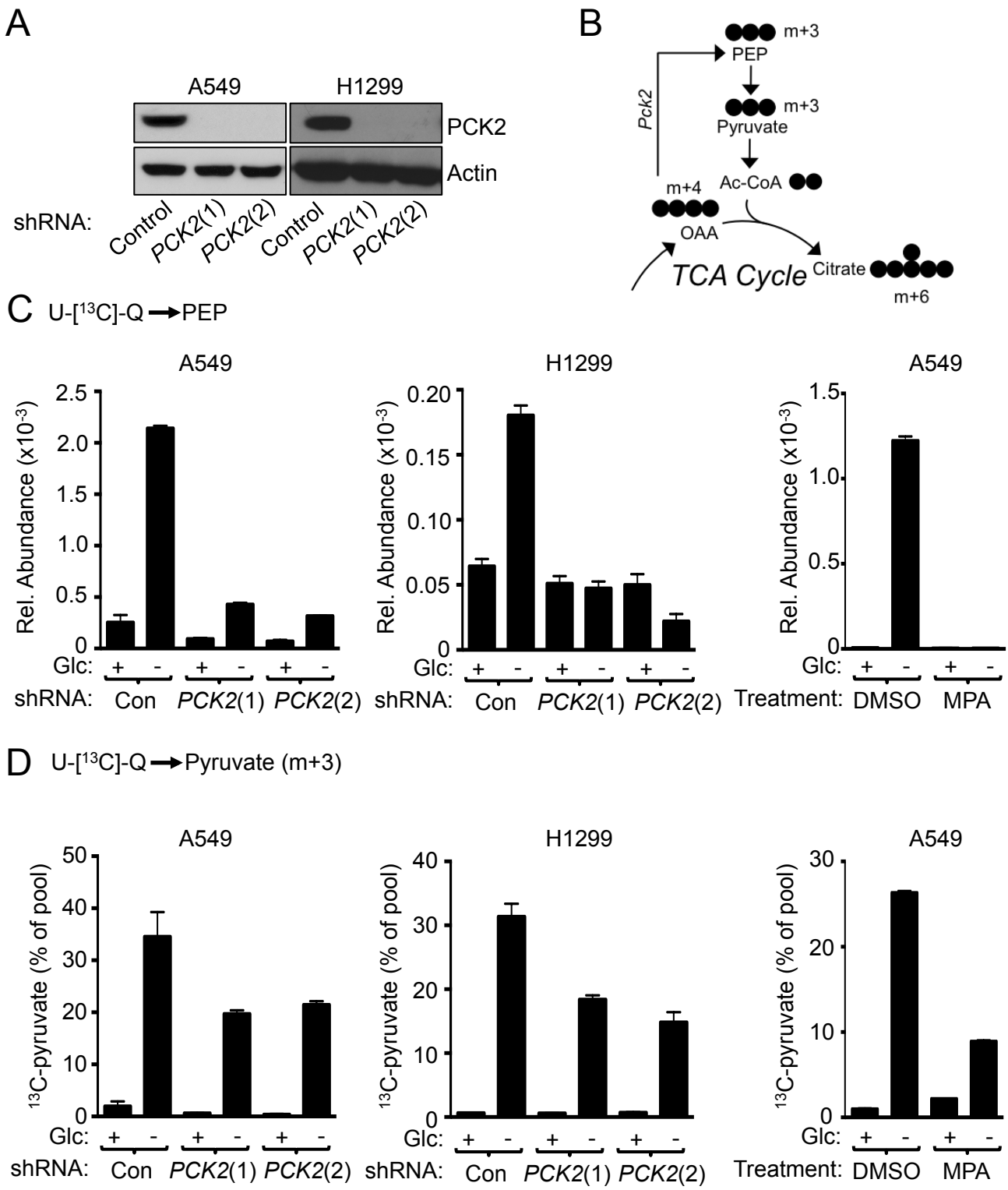
A
A549
H1299
PCK2
Actin
shRNA:
Control
PCK2(1)
PCK2(2)
Control
PCK2(1)
PCK2(2)
B
m+3
PEP
Pck2
m+3
Pyruvate
Ac-CoA
m+4
OAA
TCA Cycle
Citrate
m+6
C U-[13C]-Q → PEP
A549
H1299
A549
Rel. Abundance (x10-3)
Glc:
shRNA:
Con
PCK2(1)
PCK2(2)
Treatment:
DMSO
MPA
D U-[13C]-Q → Pyruvate (m+3)
13C-pyruvate (% of pool)

Vincent_Fig4

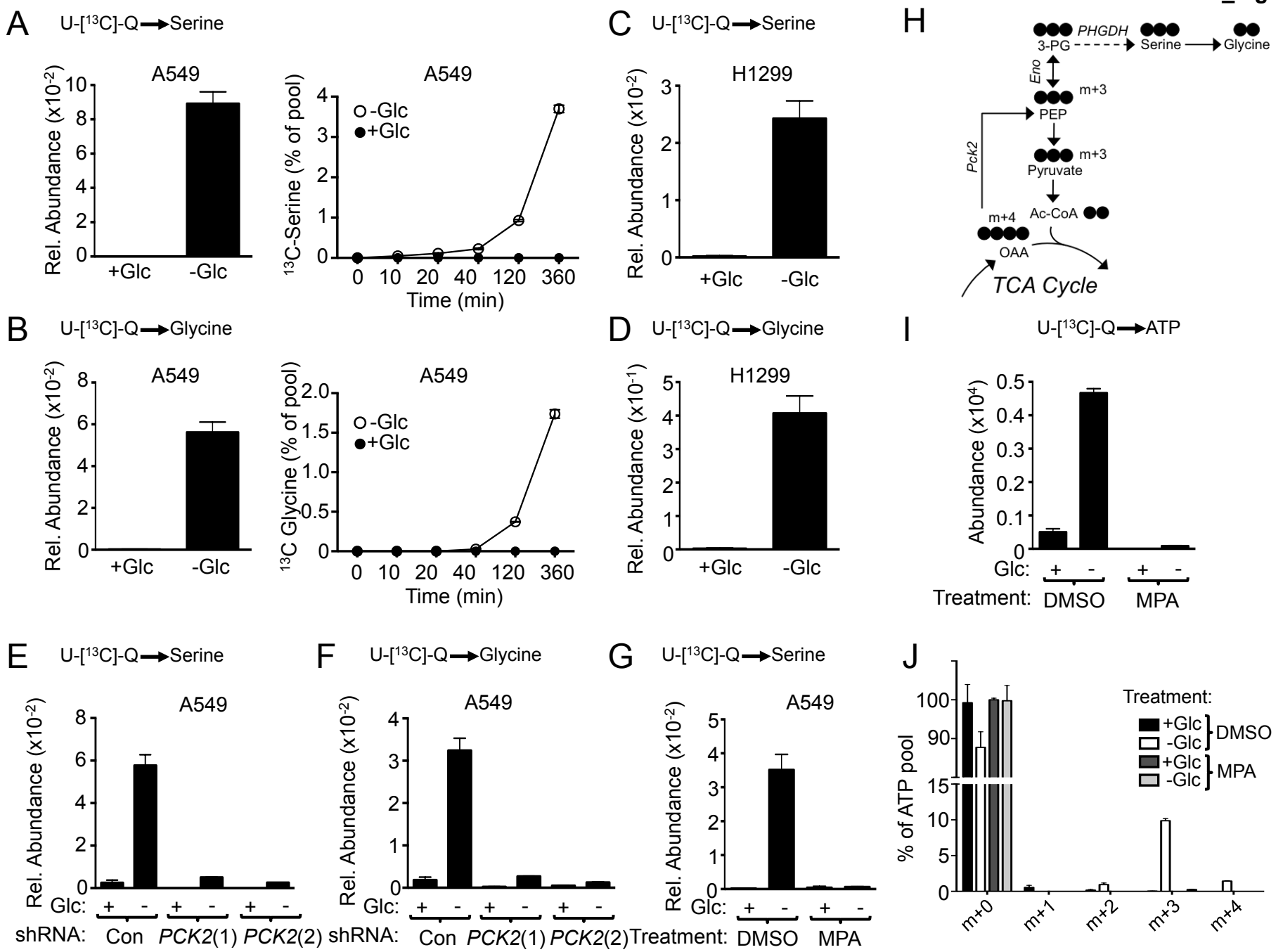

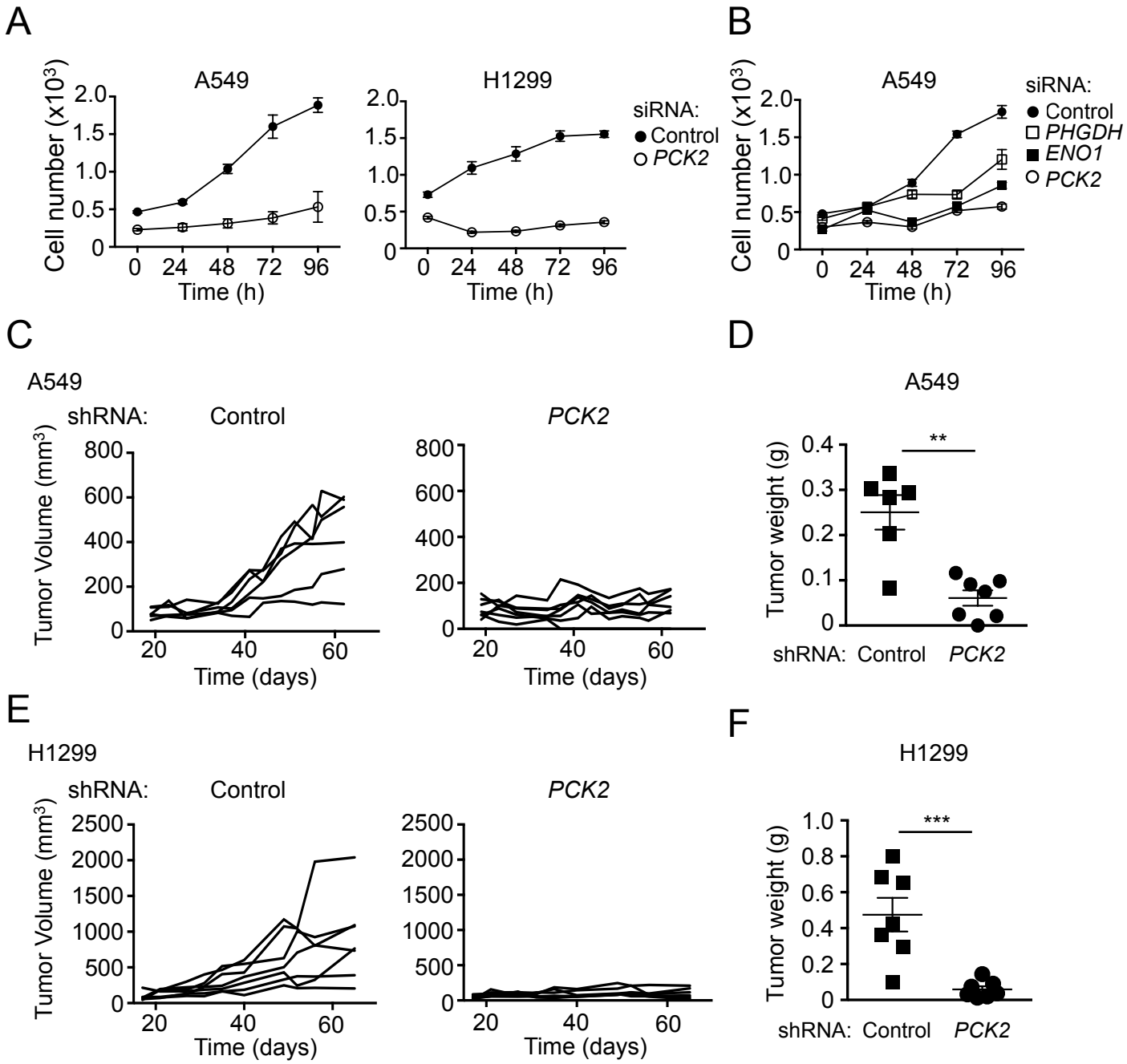
A
A549
H1299
Cell number (x10^3)
Time (h)
siRNA:
Control
PCK2
B
A549
siRNA:
Control
PHGDH
ENO1
PCK2
C
A549
shRNA:
Control
PCK2
Tumor Volume (mm^3)
Time (days)
D
A549
Tumor weight (g)
**
shRNA: Control PCK2
E
H1299
F
H1299
***

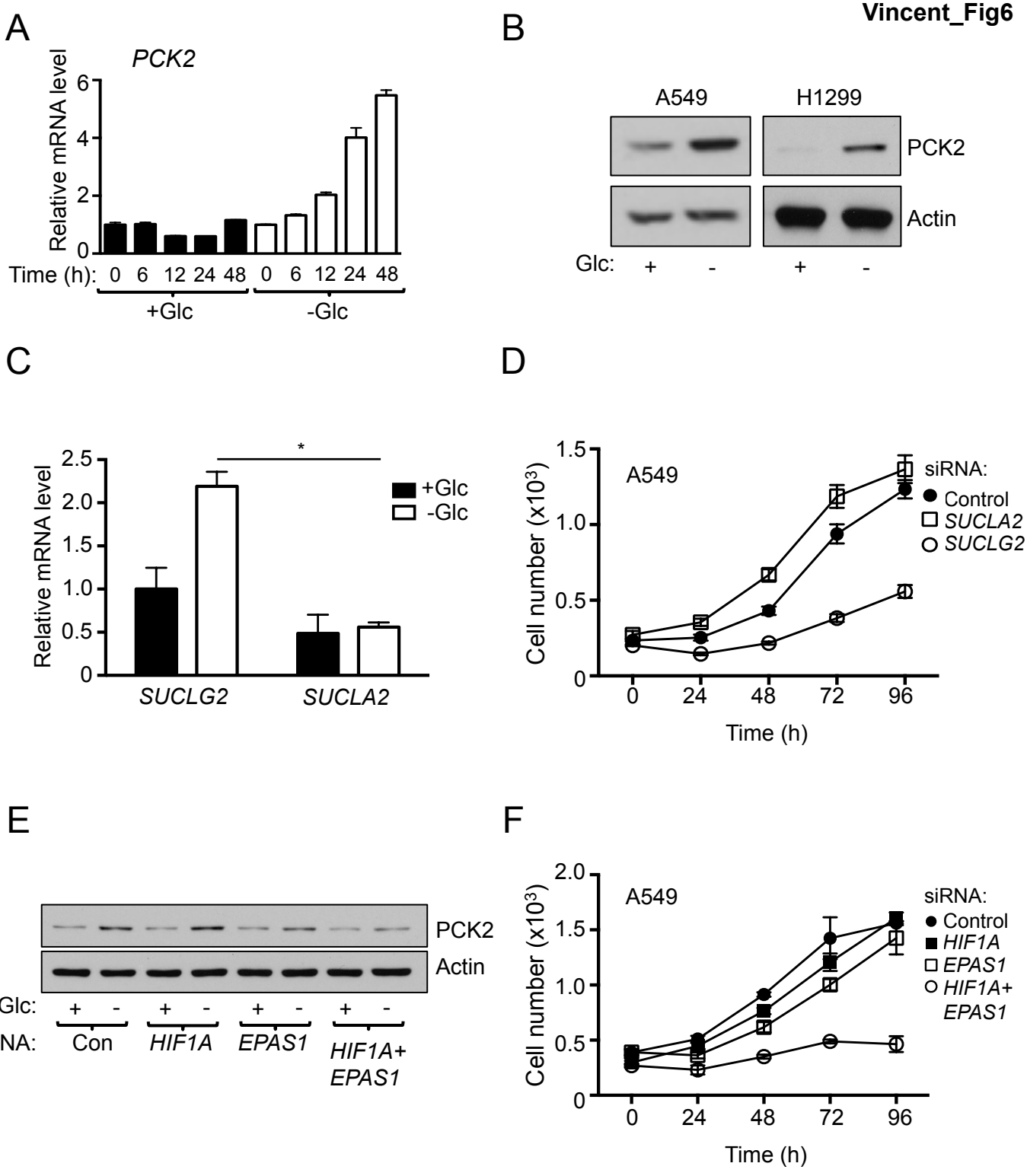
A
PCK2
Relative mRNA level
6
4
2
0
Time (h): 0 6 12 24 48 0 6 12 24 48
+Glc
-Glc
B
A549
H1299
PCK2
Actin
Glc: + - + -
C
Relative mRNA level
2.5
2.0
1.5
1.0
0.5
0
*
+Glc
-Glc
SUCLG2
SUCLA2
D
A549
Cell number (x10³)
1.5
1.0
0.5
0
0 24 48 72 96
Time (h)
siRNA:
Control
SUCLA2
SUCLG2
E
PCK2
Actin
Glc: + - + - + - + -
siRNA: Con HIF1A EPAS1 HIF1A+ EPAS1
F
A549
Cell number (x10³)
2.0
1.5
1.0
0.5
0
0 24 48 72 96
Time (h)
siRNA:
Control
HIF1A
EPAS1
HIF1A+ EPAS1

Vincent_Fig7

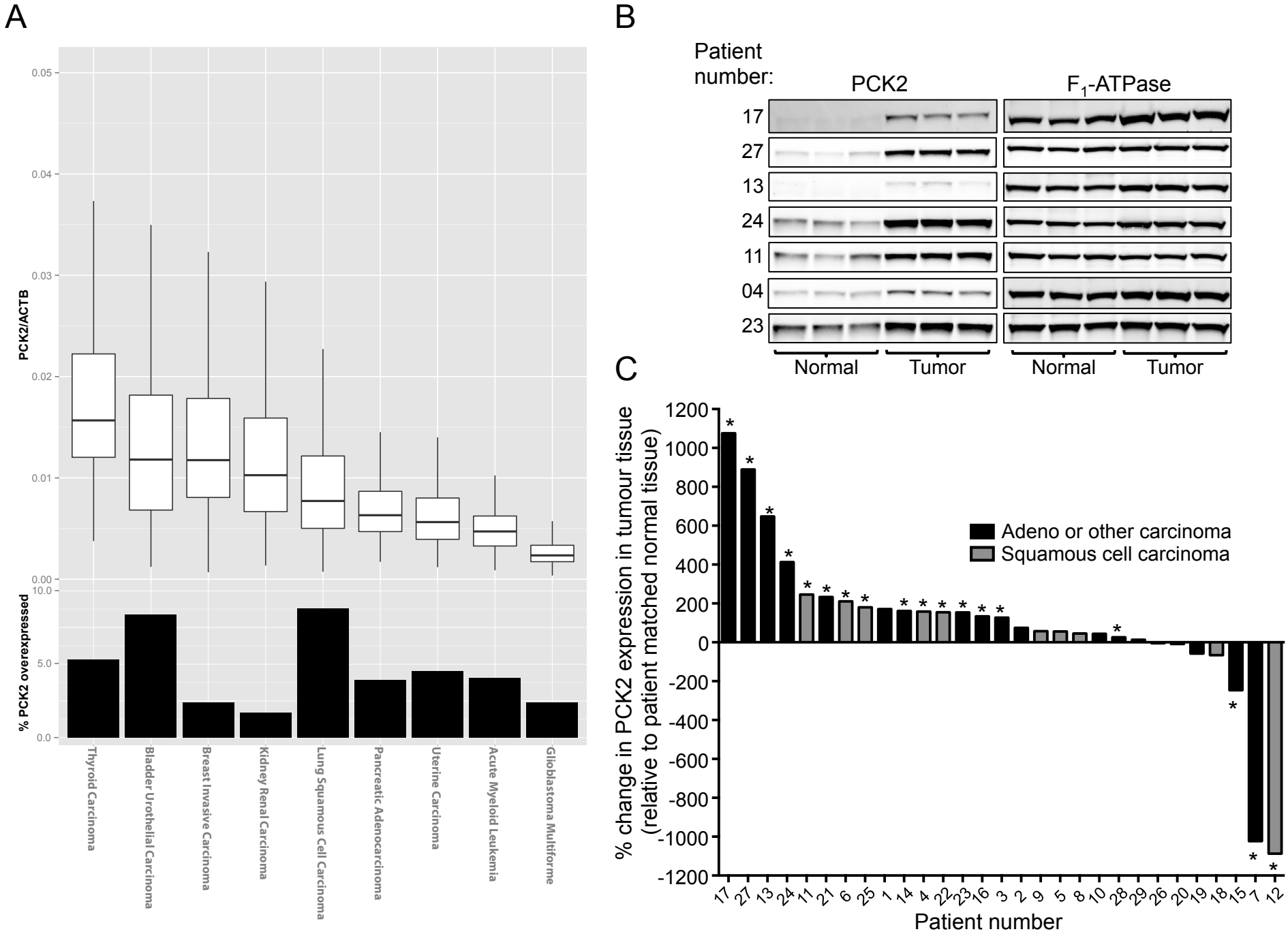

Inventory of Supplemental Information:

Figure S1, related to Fig. 1. Metabolite analysis of A549 cells grown in the absence of glucose

Vincent_FigS1

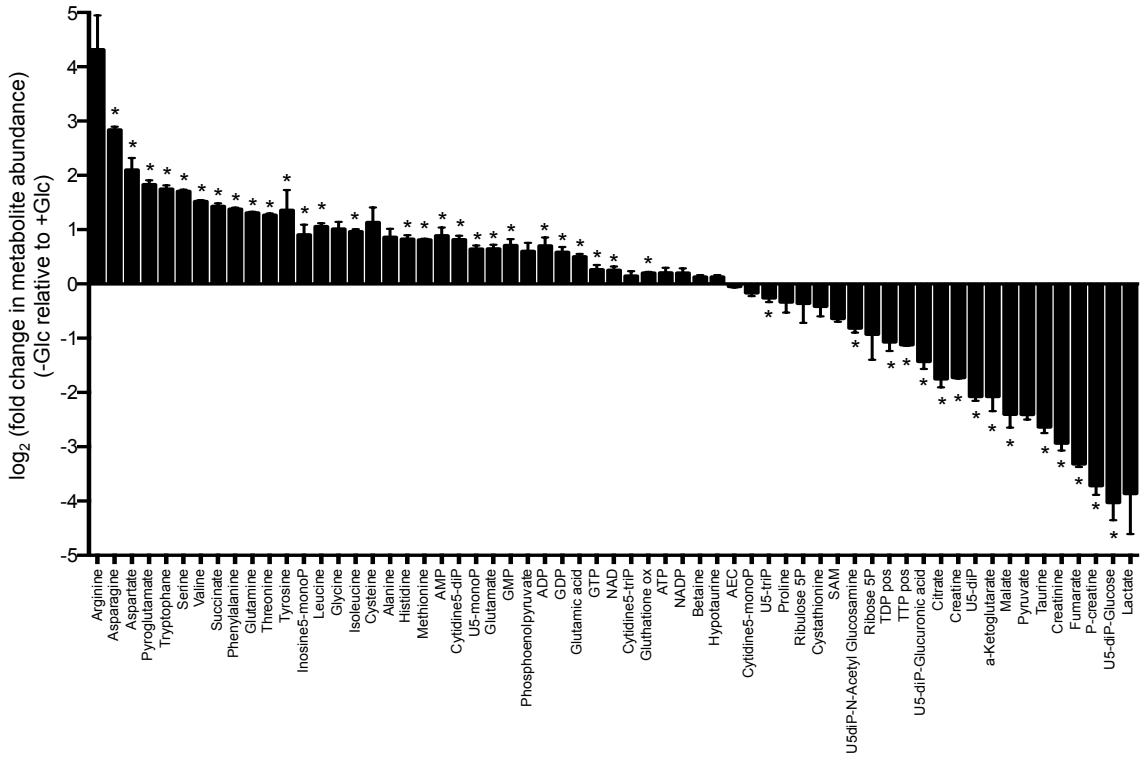

Figure S2, related to Fig. 2. Glucose withdrawal redirects glutamine metabolism to maintain the TCA cycle and for the production of PEP.

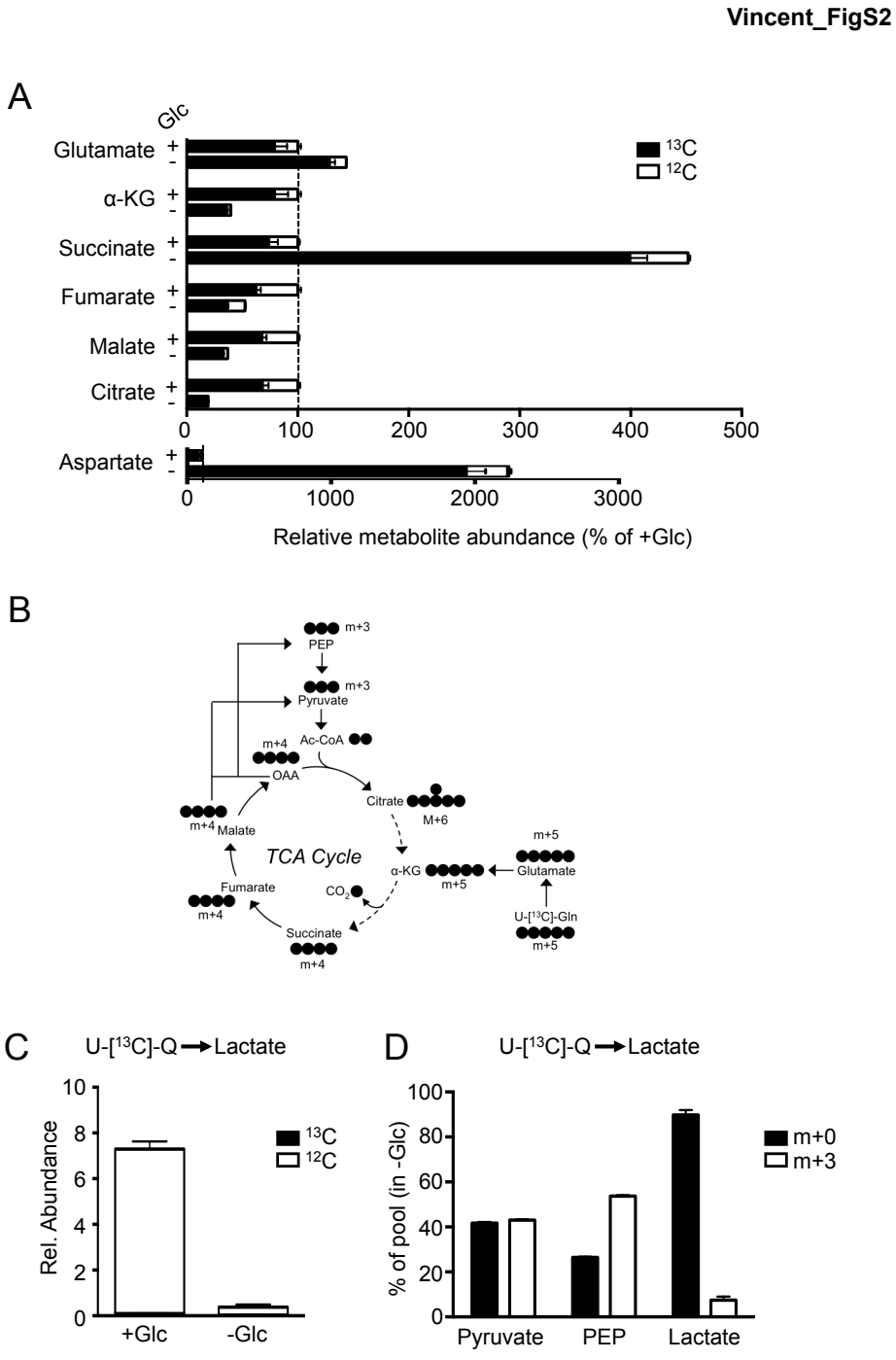

Figure S3, related to Fig. 3. TCA cycle metabolism in the absence of PCK2.

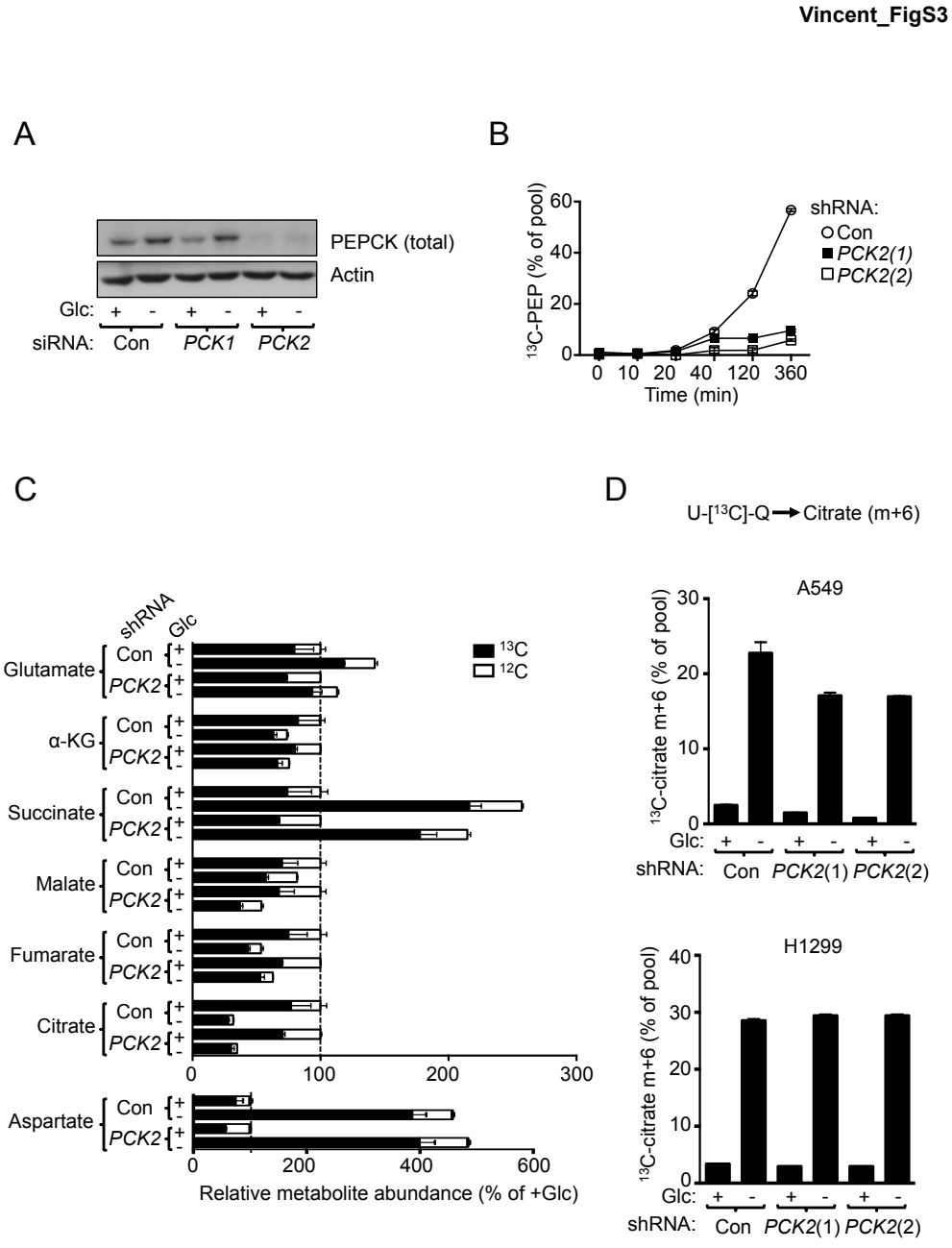

Figure S4, related to Fig. 4. Serine, glycine and ATP are made from glutamine upon glucose withdrawal in a PCK2-dependent manner.

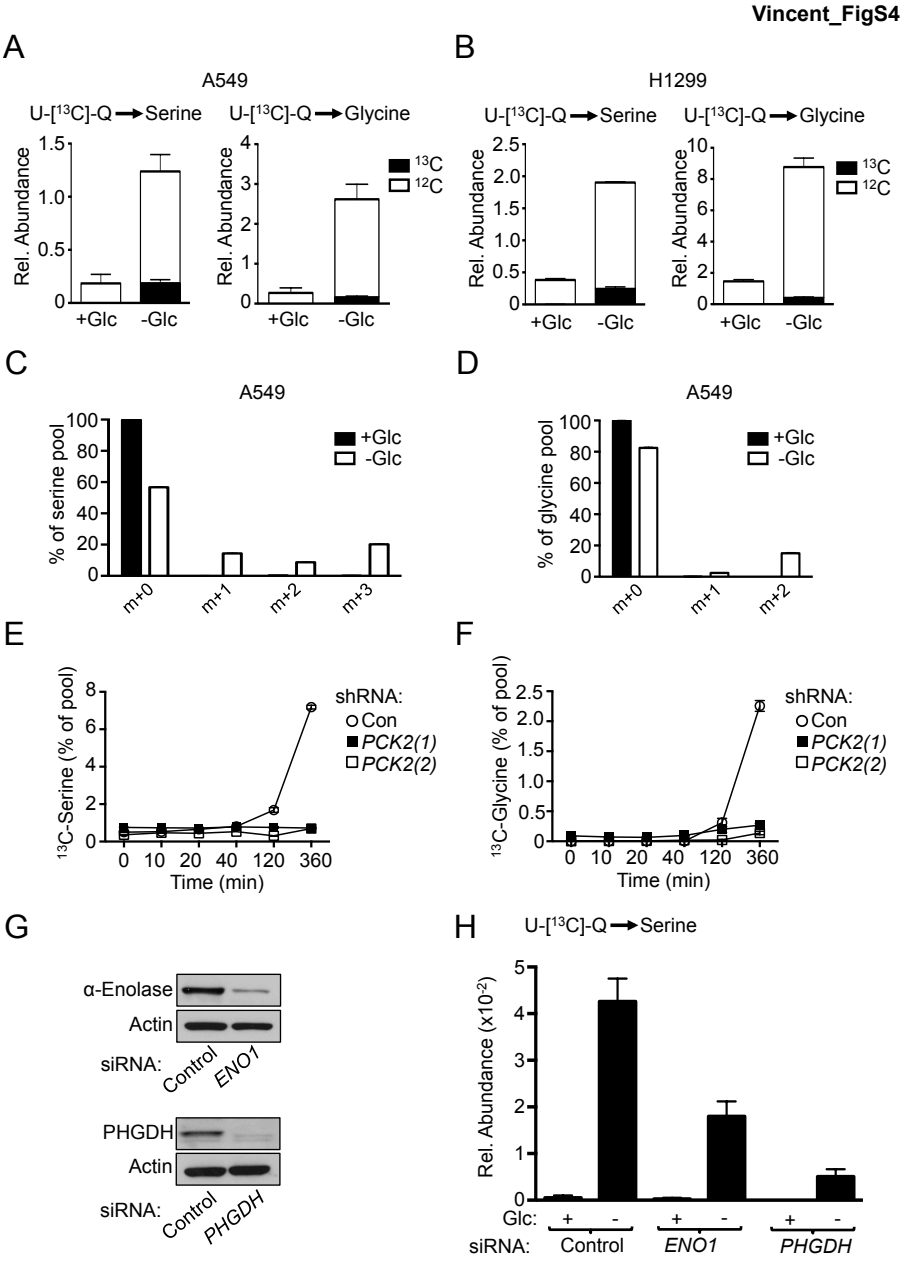

Figure S5, related to Fig. 5. Cancer cells require PCK2 to maintain glucose-independent proliferation and tumor growth *in vivo*.

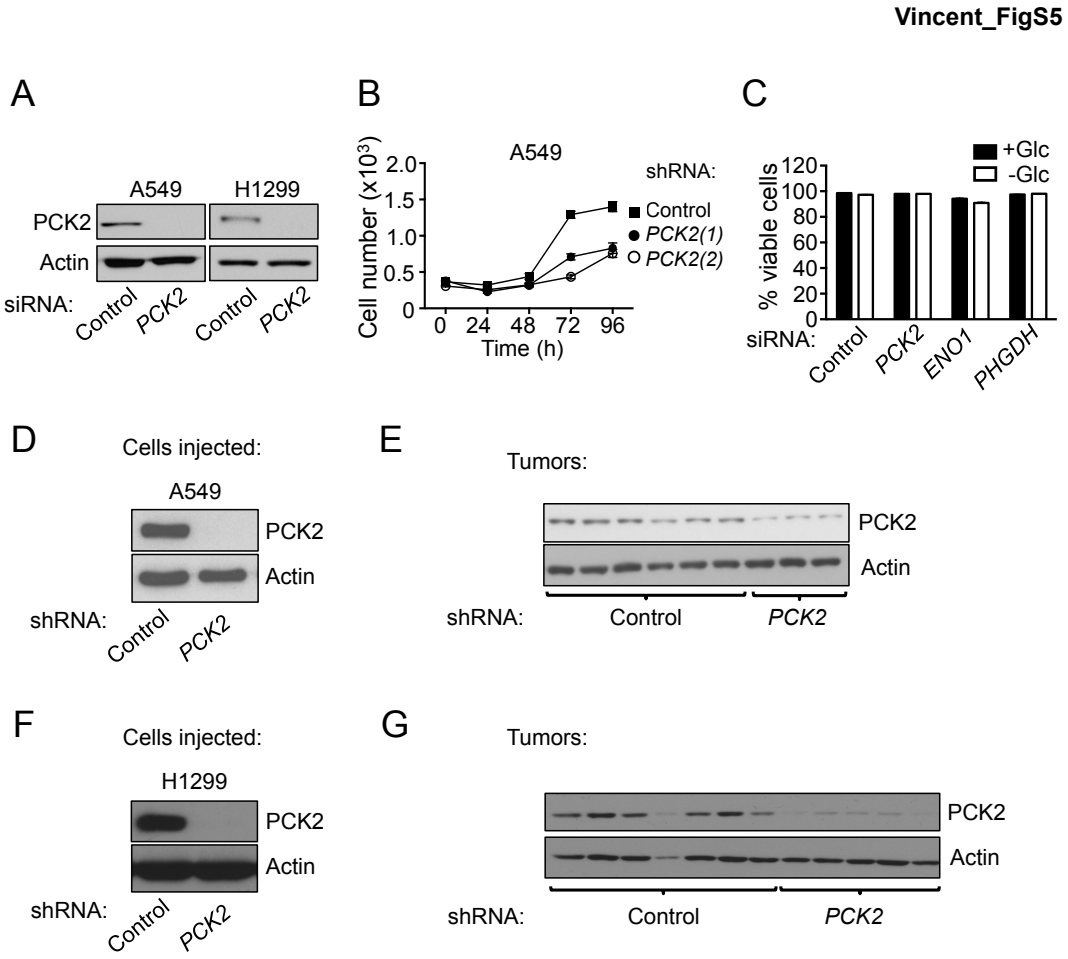

Figure S6, related to Fig. 6. PCK2 expression is regulated by glucose availability.

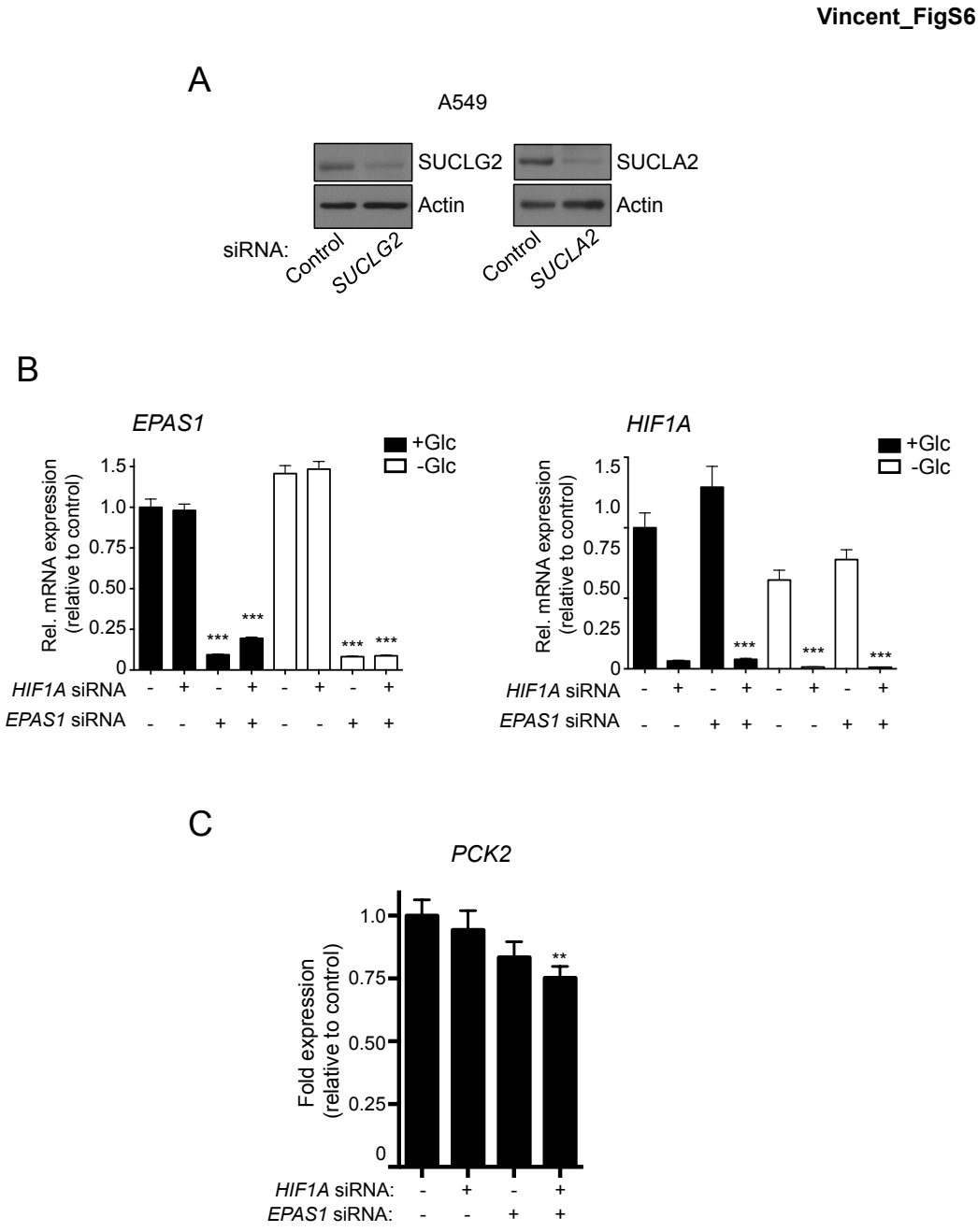

Figure S7, related to Fig.7. PCK2 expression is increased in NSCLC.

Vincent_FigS7

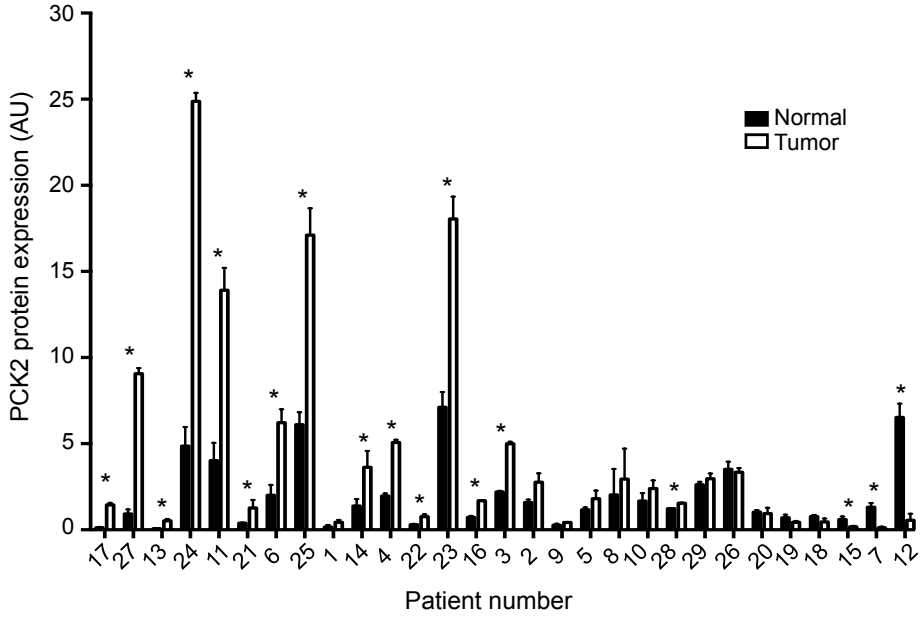

Supplementary Figure Legends:

Figure S1, related to Fig. 1. Metabolite analysis of A549 cells grown in the absence of glucose.

A549 cells were cultured in the presence (+Glc) or absence of glucose (-Glc) for 48h and metabolite abundances determined using both LC- and GC-MS. The data are displayed as the $\log_2$ of the fold change in metabolite abundance between –Glc relative to +Glc conditions. Data are represented as mean +/- SEM of three independent cultures.

Figure S2, related to Fig. 2. Glucose withdrawal redirects glutamine metabolism to maintain the TCA cycle and for the production of PEP.

(A) Relative abundances of glutamate, α-KG, succinate, fumarate, malate, citrate and aspartate after culture of A549 cells for 12h in the presence or absence of unlabeled glucose (Glc). Cells were cultured with U-[^{13}C]-Q for the last 6h of the 12h incubation. Data are presented relative to metabolite abundance in glucose-replete conditions (+Glc).

(B) Model for U-[^{13}C]-Q flux in the TCA cycle under glucose withdrawal. In the absence of glucose fully labeled TCA cycle intermediates made from U-[^{13}C]-Q can be used to make fully labeled pyruvate and PEP (m+3). Pyruvate m+3 can re-enter the TCA cycle, as acetyl-CoA (m+2), which condenses with fully labeled OAA (m+4) to give citrate m+6. Abbreviation: PEP, phosphoenolpyruvate.

(C) Relative abundance of lactate in A549 cells cultured with U-[^{13}C]-Q as in (A).

(D) The contribution of mass isotopologues (unlabeled m+0 or fully-labeled m+3) to the total pyruvate, PEP and lactate pools in A549 cells cultured with U-[^{13}C]-Q as in (A).

Data are represented as mean +/- SEM of three independent cultures.

Figure S3, related to Fig. 3. TCA cycle metabolism in the absence of PCK2.

(A) Immunoblot for total PEPCK and actin on lysates from A549 cells transfected with either control siRNA or siRNA targeting either *PCK1* or *PCK2*. Cells were incubated in the presence or absence of glucose for 48h.

(B) Contribution of U-[^{13}C]-Q to PEP in A549 cells expressing either control shRNA or shRNA targeting *PCK2* in glucose free conditions. Cells were pre-incubated in the absence of glucose for 6h before incubation with U-[^{13}C]-Q (time 0). Cells extracts were harvested at the time points shown.

(C) Relative abundances of glutamate, α-KG, succinate, fumarate, malate, citrate and aspartate in A549 cells expressing control or *PCK2* shRNA. Cells were cultured in the presence or absence of unlabeled glucose for 12h, and cultured with U-[^{13}C]-Q for the last 6h of the 12h incubation. Data are made relative to metabolite abundance in glucose-replete conditions (+Glc).

(D) Proportion of mass isotopologue citrate m+6 in A549 and H1299 cells expressing control or *PCK2* shRNA. Cells were cultured in the presence or absence of glucose as in (C).

(B-D) Data are represented as mean +/- SEM of three independent cultures.

Figure S4, related to Fig. 4. Serine, glycine and ATP are made from glutamine upon glucose withdrawal in a PCK2-dependent manner.

(A-B) Relative abundances of serine and glycine and the contribution of U-[^{13}C]-Q to these metabolites in A549 cells (A) or H1299 cells (B). Cells were cultured in the absence or presence of unlabeled glucose for 12h, with U-[^{13}C]-Q being present for the last 6h of the 12h incubation.

(C-D) Contribution of the mass isotopologues of serine (C) and glycine (D) to the total metabolite pool in A549 cells. Cells were incubated with U-[^{13}C]-Q in the presence or absence of glucose for 48h before cells extracts were harvested.

(E-F) Contribution of U-[^{13}C]-Q to serine (E) and glycine (F) in A549 cells expressing either control shRNA or shRNA targeting *PCK2* in glucose free conditions. Cells were pre-incubated in the absence of glucose for 6h before incubation with U-[^{13}C]-Q (time 0). Cells extracts were harvested at the time points shown.

(G) Immunoblot for enolase, PHGDH and actin on lysates from A549 cells 3 days post transfection with either control siRNA or siRNA targeting either *ENO1* or *PHGDH*.

(H) Relative abundance of ^{13}C-serine in A549 cells transfected with either control siRNA or siRNA targeting either *ENO1* or *PHGDH*. Cells were cultured as in (A).

(A-F and H) Data are represented as mean +/- SEM of three independent cultures

Figure S5, related to Fig. 5. Cancer cells require PCK2 to maintain glucose-independent proliferation and tumor growth *in vivo*.

(A) Immunoblot for PCK2 and actin on lysates from A549 and H1299 cells 3 days post transfection with either control siRNA or siRNA targeting *PCK2*.

(B) Proliferation of A549 cells expressing either control shRNA or shRNA targeting *PCK2* in glucose-free media over 96 hours. Data are represented as mean +/- SEM for biological replicates (n=5).

(C) A549 cells transfected with siRNA targeting *PCK2*, *ENO1* or *PHGDH* were cultured for 48h in the presence or absence of glucose before staining with propidium iodide to measure the percentage of viable cells. Data are represented as mean +/- SEM of three independent cultures.

(D-G) Immunoblot for PCK2 and actin on lysates from A549 (D) and H1299 (F) cells, expressing either control or shRNA targeting *PCK2,* injected into the flanks of nude mice. Immunoblot for PCK2 and actin on lysates from the resulting tumors (where enough tissue was available) formed from the A549 (E) and H1299 (G) cells injected.

Figure S6, related to Fig. 6. PCK2 expression is regulated by glucose availability.

(A) Immunoblot for SUCLG2, SUCLA2 and actin on lysates from A549 cells 3 days post transfection with either control siRNA or siRNA targeting either *SUCLG2* or *SUCLA2*.

(B) Expression of *HIF1A* and *EPAS1* mRNA in A549 cells. A549 cells transfected with control siRNA or siRNA targeting *HIF1A*, *EPAS1* or a combination of both were incubated in the presence or absence of glucose for 48h. Transcript levels for *HIF1A* or *EPAS1* mRNA were determined relative to *OGDH* mRNA levels, and normalized relative to control cells (transfected with control siRNA). ***, $p<0.001$.

(C) Relative expression of *PCK2* mRNA as determined by qPCR. A549 cells transfected with siRNA against *HIF1A*, *EPAS1* or a combination of both were cultured in the presence or absence of glucose for 48h. PCK2 mRNA transcript levels were determined relative to *OGDH* mRNA levels, and normalized relative to expression in cells transfected with control siRNA. **, $p<0.01$.

(B-C) Data are represented as mean +/- SEM of three independent cultures.

Figure S7, related to Fig.7. PCK2 expression is increased in NSCLC.

Quantified proteomic data from 29 NSCLC patients. Each bar represents the average expression of PCK2 in 3 pieces of normal tissue (black bars) or 3 pieces of tumour tissue (white bars) for

each patient (mean +/- SEM). The strength of evidence for a difference in expression between the normal and tumour samples was determined by a Kruskal-Wallis test, *, $p<0.05$.

Table S1: List of qPCR primers

Gene	Forward Primer	Reverse Primer
PCK2	TGCCAGGCTGGAAAGTGGAGTGT	GCAACCCCAAAGAAGCCGTTCTCA
HIF1A	TGCTCATCAGTTGCCACTTCC	CGCTGTGTGTTTTGTTCTTTACCC
EPAS1	GCCTCCATCATGCGACTGGCA	CCATCTTGGGTCACCACGGCA
OGDH	AGACCCCTGGGATCATGCAGTTCA	CCTCGCAGCCTTCTAGACCAAAGC
PCK1	CTGTGACGGCTCTGAGGAGGAGAA	CCACATCCCTGGGGTCAGTGAGAG

Supplementary Experimental Procedures:

Materials

The PEPCK inhibitor 3-mercaptopicolinic acid (MPA) was obtained from Santa Cruz Biotechnology (Dallas, TX, USA). Primary antibodies to PCK2 and actin, as well as HRP-conjugated anti-rabbit and anti-mouse secondary antibodies were obtained from Cell Signaling Technology (Danvers, MA, USA). Primary antibody to α-enolase was obtained from Santa Cruz Biotechnology (Dallas, TX, USA). PHGDH antibodies were obtained from Thermo Fisher (Waltham, MA, USA). Primary antibodies to SUCLG2 and SUCLA2 were obtained from Novus Biologicals (Littleton, CO, USA).

Cell culture

A549 and H1299 cell lines were obtained from ATCC (Manassas, VA, USA). Cells were cultured in 'growth medium' (DMEM (A549 cells) or RPMI (H1299 cells)) supplemented with 10% fetal bovine serum (FBS), 20000U/ml penicillin, 7mM streptomycin and 2mM glutamine and non-essential amino acids (for H1299 cells). Cells were grown at 37°C in a humidified atmosphere supplemented with 5% (v/v) CO_2. For experiments cells were cultured in DMEM with 20000U/ml penicillin, 7mM streptomycin and 10% dialysed FBS (Wisent, Saint-John-Baptiste, QC, Canada), 2mM glutamine and 25mM glucose were then added as required.

shRNA and siRNA knockdown

PCK2 knockdown was achieved using lentiviral shRNA vectors (ID numbers: TRCN0000052664 and TRCN0000052666) from the TRC shRNA collection (Sigma-Aldrich, St. Louis, MO). Lentiviral supernatants were generated as described (Huang et al., 2012). All transient

knockdowns in this manuscript were achieved using the SMARTpool ON-TARGETplus siRNA reagent (composed of 4 individual siRNAs for each target) from GE Dharmacon (Layette, CO, USA). 50nM siRNA was incubated for 20min with RNAimax in OptiMEM medium (Life Technologies) in a 12 well plate, followed by seeding of cells (60,000 cells/well). Cells were transfected a second time 48 hours later, and cells plated for assays the following day.

RNA-Seq analysis

A549 cells were cultured in the presence (25 mM) or absence of glucose for 48 hours prior to RNA extraction. For cDNA synthesis, custom oligo-dT primers were used with a barcode and adapter-linker sequence (CCTACACGACGCTCTTCCGATCT—XXXXXXXX-T15). After first strand synthesis, samples were pooled together based on *ACTB* qPCR values, and RNA-DNA hybrids degraded using consecutive acid-alkali treatment. A second sequencing linker (AGATCGGAAGAGCACACGTCTG) was ligated using T4 ligase (NEB) followed by SPRI clean-up. The mixture was then PCR enriched for 12 cycles and SPRI purified to yield final strand specific RNA-seq libraries as previously described (Jha et al., 2015). Libraries were sequenced using a HiSeq 2500 (Illumina) using 50bpX25bp pair-end sequencing. Second mate was used for sample demultiplexing, at which point individual single-end fastqs were aligned to mm9 genome using TopHat. and gene expression was obtained using ht-seq and DESeq2 for differential expression. Raw and processed sequencing data are deposited at Pubmed GEO under GSE66556.

Metabolite profiling by LC-MS

Liquid chromatography was performed using a 1290 Infinity ultra-performance LC system (Agilent Technologies, Santa Clara, CA, USA) equipped with a Scherzo 3 μm, 3.0×150mm SM-C18 column (Imtakt Corp, Japan). The column temperature was maintained at 10°C and the mobile phases A and B consisted of water containing 5 and 200mM ammonium acetate, respectively. The chromatographic gradient started at 100% mobile phase (A) with a 5 min gradient to 100% (B). This was followed by a 5min hold time at 100% mobile phase B at a flow rate of 0.4ml/min. A subsequent re-equilibration time (6min) was performed before the next injection. Sample volumes of 5μl were injected for LC-MS analysis. LC-MS analysis was performed on an Agilent 6540 UHD Accurate-Mass Q-TOF mass spectrometer (Agilent Technologies, Santa Clara, CA, USA). Analyte ionization was accomplished using an electrospray ionization source (ESI) in both positive and negative polarities. The source operating conditions were set at 325°C and 9l/min for gas temperature and flow respectively, nebulizer pressure was set at 40psi and capillary voltage was set a 4.0kV. Reference masses 121.0509, 922.0099, 1033.9881 were introduced into the source through a secondary spray nozzle to ensure accurate mass. MS data were acquired in full scan mode mass range: m/z 100-1000; scan time: 1.4s; data collection: centroid and profile. Retention times, and accurate mass for each compound were confirmed against authentic standards as well as matched unlabeled cell extracts grown under the same conditions when cells were undergoing stable isotope tracer analysis (SITA). Data were quantified by integrating the area underneath the curve of each compound using MassHunter Qual (Agilent Technologies, Santa Clara, CA, USA). Each metabolite's accurate mass ion and subsequent isotopic ions were extracted (EIC) using a 10 ppm window.

Network-based data integration

Network-based integration of metabolite and gene expression datasets was conducted as previously described (Jha et al., 2015). A chemical mapping table between carbon atoms in substrates and products for all annotated reactions in the KEGG database using RPAIRs entries was made (Kanehisa et al., 2012). Only those atoms that could be uniquely identified by the chemical structure (i.e. constant between different stereoisomers) were used. Using such a chemical mapping table we built a network of individual carbon atoms connected by a substrate-product relationship via biochemical reactions. Each metabolite is present in the network through a number of disconnected nodes representing individual carbon atoms within the metabolite, with common metabolites (i.e. water, ATP, NAD) removed from the network to avoid redundancy. At the final filtering stage only reactions catalyzed by enzymes with significant expression levels were kept. The top 12000 expressed genes were used as a cutoff, to generate a network containing approximately 6000 nodes and 6000 edges.

To search for sub-networks upregulated by glucose deprivation, network nodes and edges were assigned a score by differential expression analysis using DESeq2 (Love et al., 2014). The actual score was a sum of $\log_2$ mean gene expression and value of DE test statistic minus a threshold value that was a parameter to reflect importance of both basal expression level and differential regulation of the enzyme. To assign a score to the nodes, we performed a t-test on metabolite levels in two conditions, and used the logarithm of the *p*-value as the node score. Metabolites that were not measured had a score of zero. In the scored network we used a heuristic algorithm to find the most connected sub-network with maximal total node and edge scores. Threshold values were selected to create a sub-network with 100-150 metabolites. This sub-network was then enriched in reaction edges, connecting the metabolites provided the corresponding enzymes were highly expressed (top 6000 by expression, irrespective of their

differential expression). Finally multiple atoms of the same compound were collapsed to yield a network containing a single node for each compound to ease visualization and interpretation.

NSCLC patients and tissue samples

The study was approved by the local research ethics committee: UK National South West 4 Research Ethics Committee (REC) Southmead Hospital, Bristol BS10 5NB. REC no: 07/Q2002/6, South West 4 REC.

Three distinct samples of the tumour and adjacent normal tissue from the resection margin were taken, flash frozen in liquid nitrogen, and stored at −80°C until further analysis. Only those NSCLC tumour samples comprising at least 90% tumour tissue were analyzed. Frozen tissue samples were homogenized and extracted as previously described. Briefly, a Polytron homogenizer was used to generate tissue lysates in 1% NP40 lysis buffer. Protein concentration was determined by BCA assay (Thermo Scientific, IL, USA) and tissue lysates were stored at −80°C.

Supplementary References:

Huang, S., Holzel, M., Knijnenburg, T., Schlicker, A., Roepman, P., McDermott, U., Garnett, M., Grernrum, W., Sun, C., Prahallad, A.*, et al.* (2012). MED12 controls the response to multiple cancer drugs through regulation of TGF-beta receptor signaling. Cell *151*, 937-950.

Jha, A.K., Huang, S.C.-C., Sergushichev, A., Lampropoulou, V., Ivanova, Y., Loginicheva, E., Chmielewski, K., Stewart, K.M., Ashall, J., Everts, B.*, et al.* (2015). Network integration of parallel metabolomic-transcriptional data reveals novel metabolic modules regulating divergent macrophage polarization. Immunity *42*, 419-430.

Kanehisa, M., Goto, S., Sato, Y., Furumichi, M., and Tanabe, M. (2012). KEGG for integration and interpretation of large-scale molecular data sets. Nucleic acids research *40*, D109-114.

Love, M.I., Huber, W., and Anders, S. (2014). Moderated estimation of fold change and dispersion for RNA-seq data with DESeq2. Genome Biol *15*, 550.